Multiphoton Processes, Entanglement and Quantum Walk in Hybrid Systems: Circuit QED and Nitrogen Vacancy Centers

by

Ali Ümit Cemal Hardal

Submitted to the Graduate School of Sciences and Engineering
in partial fulfillment of the requirements for the degree of

Doctor of Philosophy in Physics

at the

KOÇ UNIVERSITY

September 2014

September 2014

Koc University

Graduate School of Sciences and Engineering

This is to certify that I have examined this copy of a doctoral thesis by

Ali Ümit Cemal Hardal

and have found that it is complete and satisfactory in all respects,
and that any and all revisions required by the final
examining committee have been made.

Committee Members:

Prof. Dr. Özgür E. Müstecaplıoğlu (Advisor)

Prof. Dr. Tekin Dereli

Assoc. Prof. Dr. Zafer Gedik

Assist. Prof. Dr. Alkan Kabakçıoğlu

Assist. Prof. Dr. Şükrü E. Kocabaş

Date:

Multiphoton Processes, Entanglement and Quantum Walk in Hybrid Systems: Circuit QED and Nitrogen Vacancy Centers

by

Ali Ümit Cemal Hardal

Submitted to the Graduate School of Sciences and Engineering
in partial fulfillment of the requirements for the degree of
Doctor of Philosophy in Physics

Abstract

In this thesis, we first examine transfer of particle entanglement and spin squeezing between atomic and photonic subsystems in optical cavities coupled by two-photon exchange. Each cavity contains a single atom, interacting with cavity photons with a two-photon cascade transition. Particle entanglement is characterized by evaluating optimal spin squeezing inequalities for the cases of initially separable and entangled two-photon states. It is found that particle entanglement is first generated among the photons in separate cavities and then transferred to the atoms. The underlying mechanism is recognized as an intercavity two-axis twisting spin squeezing interaction, induced by two-photon exchange, and its optimal combination with the intracavity atom-photon coupling. Secondly, we investigate spin squeezing, quantum entanglement, and second-order coherence in two coupled, driven, dissipative, nonlinear cavities. Solving the quantum optical master equation of the system numerically in the steady state, we calculate the zero-time delay second-order correlation function for the coherent, genuine two-mode entanglement parameters, an optimal spin squeezing inequality associated with particle entanglement, concurrence, quantum entropy, and logarithmic negativity. We compare these quantum statistical properties for the cavities coupled with either single- or two-photon exchange. In the final part of the thesis, we propose a quantum-electrodynamics scheme for implementing the discrete-time, coined quantum walk with the walker corresponding to the phase degree of freedom for a quasimagnon field realized in an ensemble of nitrogen-vacancy centers in diamond. The coin is realized as a superconducting flux qubit. Our scheme improves on an existing proposal for implementing quantum walks in cavity quantum electrodynamics by removing the cumbersome requirement of varying drive-pulse durations according to mean quasiparticle number.

Özet

Bu tezde ilk olarak, 2-foton değişimi ile birleştirilmiş optiksel kavitelerde, atom ve foton alt sistemleri arasında ki parçacık dolanıklılığı ve spin sıkışması transferleri incelenmiştir. Her bir kavitede, kavite fotonları ile 2-foton basamak geçişleri aracılığı ile etkileşen tek bir atom bulunur. Parçacık dolanıklılığı, ilk durumları ayrık ve dolanık 2-foton durumları için, optimal spin sıkışması eşitsizlikleri aracılığı ile incelenmiştir. Parçacık dolanıklılığının ilk olarak ayrık kavitelerdeki fotonlar arasında oluştuğu ve daha sonra atomlara aktarıldığı bulunmuştur. Temel fiziksel mekanizmanın 2-foton ile indüklenen 2-eksen burulma spin sıkıştırma etkileşimi ile atom-foton etkileşim gücünün optimal bir kombinasyonu olduğu anlaşılmıştır. İkinci olarak, iki tane birleştirilmiş, sürülmüş, yitirgen ve doğrusal olmayan kavitelerde spin sıkışması, kuantum dolanıklılık ve optiksel koherent incelenmiştir. İkinci-derece korelasyon parametresi, iki-kip dolanıklılık parametreleri, bir optimal spin sıkışması eşitsizliği, uyuşum parametresi, kuantum etropisi ve logaritmik negativite, kuantum optiksel master denklemi çözülerek durağan durumda incelenmiştir. Bu istatiksel nicelikler 1- ve 2-foton değişimi durumları için birbirleri ile kıyaslanmıştır. Son olarak, süreksiz kuantum yürüyüşleri için kuantum elektrodinamiksel bir uygulama önerilmiştir. Bu uygulamada, yürüyücüler kusurlu elmaslarda ki Nitrojen-boşluk kümelerinin kipleri ile betimlenirken, madeni parayı süperiletken akı kübiti temsil etmektedir. Önerimiz, değişken sürücü-puls zaman aralıkları içermediğinden, varolan kuantum yürüyücü modellerini geliştirmektedir.

Acknowledgments

First of all, I thank Professor Özgür Esat Müstecaplıoğlu for his guidance in the past four years. He always believed in me and shared his priceless knowledge without any expectations. He presented countless doors and helped me to engineer unique keys to open them.

I thank Professor Tekin Dereli who never gave up on me. I owe him my deepest gratitudes.

There are no words to describe how grateful I am to my family who gave me unlimited support to accomplish my dreams. They are the invisible architects who worked behind the scenes throughout the way that directed me to this point. Without them, the present thesis could not be came into existence.

I express my special gratitudes towards my beloved congenial companion Hazan Ezgi İmer. During all these stressful years of my graduate studies, she was the one who always there for me. She stood up with me and endured and shared the difficulties of the life of an academician. I will be in her debt till eternity.

This thesis is based on the following papers of the author:

1. A. Ü. C. Hardal, Ö. E. Müstecaplıoğlu, J. Opt. Soc. Am. B **31**, 1402-1409 (2014)

2. A. Ü. C. Hardal, P. Xue, Y. Shikano, Ö. E. Müstecaplıoğlu and B. C. Sanders, Phys. Rev. A **88**, 022303 (2013)

3. A. Ü. C. Hardal, Ö. E. Müstecaplıoğlu, J. Opt. Soc. Am. B **29**, 1822-1828 (2012)

Other papers of the author are:

1. A. Ü. C. Hardal, J. Opt. Soc. Am. B **31**, 2339-2344 (2014)

2. F. Altıntaş, A. Ü. C. Hardal, Ö. E. Müstecaplıoğlu, Phys. Rev. E **90**, 032102 (2014)

3. A. Ü. C. Hardal, Ö. E. Müstecaplıoğlu, Phys. Scr. T **160**, 4016 (2014)

Contents

List of Figures

Chapter 1

Preliminaries

Here, we shall briefly discuss some fundamental topics which are most relevant for the present thesis. We only provide the basic understandings on the subjects and do not concern about the details. If it is necessary, we shall refer to the appropriate references.

We start with the atom-field interactions in optical cavities and discuss both the Rabi [1, 2] and the Jaynes-Cummings [3] models. We, then, proceed with the superconducting (artificial) qubits (quantum bits). We finalise this chapter with the discussions on (discrete time) quantum random walks.

1.1 Interaction of an atom with a single mode of light

Here, we shall first consider a semiclassical approach to the problem of an atom interacting with a radiation field. We shall consider so-called the minimal coupling Hamiltonian [4]

$$H = \frac{1}{2m}\left[\vec{p} - e\vec{A}(\vec{r},t)\right]^2 + eU(\vec{r},t) + V(r), \tag{1.1}$$

and make the dipole approximation. The quantum Rabi [1, 2] model which describes the interaction of a two-level atom with a single mode of light will be obtained by quantizing the electromagnetic field. We, then, finally make the rotating-wave approximation to obtain the Jaynes-Cummings model [3].

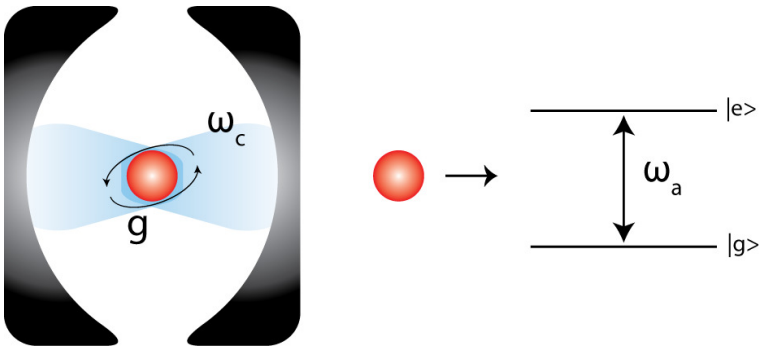

Figure 1-1: A two-level atom with transition frequency ω_a interacting with a cavity field with frequency ω_c.

1.1.1 Dipole approximation and the Rabi Model

We consider an electron bound by a potential $V(r)$ to a nucleus at the position of $\vec{r}_0$. We assume that the atom is completely immersed in a plane electromagnetic wave described by a vector potential $\vec{A}(\vec{r}_0 + \vec{r}, t)$. Now, if $\vec{k} \cdot \vec{r} \ll 1$, we can write

$$\begin{aligned}
\vec{A}(\vec{r}_0 + \vec{r}, t) &= A(t) \exp\left[i\vec{k} \cdot (\vec{r}_0 + \vec{r})\right] \\
&= A(t) \exp\left[i\vec{k} \cdot \vec{r}_0\right] \exp\left[i\vec{k} \cdot \vec{r}\right] \\
&= A(t) \exp\left[i\vec{k} \cdot \vec{r}_0\right] (1 + i\vec{k} \cdot \vec{r} + ...) \\
&\approx A(t) \exp\left[i\vec{k} \cdot \vec{r}_0\right] \\
&= \vec{A}(\vec{r}_0, t). \qquad (1.2)
\end{aligned}$$

The above approximation is called the dipole approximation and in the radiation gauge $U(\vec{r}, t) = 0$, $\vec{\nabla} \cdot \vec{A} = 0$ the Schrödinger equation reads

$$i\hbar \frac{\partial \psi(\vec{r}, t)}{\partial t} = \left\{ -\frac{\hbar^2}{2m} \left[\vec{\nabla} - \frac{ie}{\hbar} \vec{A}(\vec{r}_0, t)\right]^2 + V(r) \right\} \psi(\vec{r}, t), \qquad (1.3)$$

which can be further simplified to give [4]

$$i\hbar \dot{\phi}(\vec{r}, t) = \left[H_0 - e\vec{r} \cdot \vec{E}(\vec{r}_0, t)\right] \phi(\vec{r}, t). \qquad (1.4)$$

Here, $\cdot$ refers to the partial derivative with respect to the time, $H_0 = p^2/2m + V(r)$, $\vec{E} = -\dot{\vec{A}}$ and we define $\psi(\vec{r},t) = \exp\left[(ie/\hbar)\vec{A}(\vec{r}_0,t)\cdot\vec{r}\right]\phi(\vec{r},t)$.

We can now turn our attention to the quantum problem of a two-level atom interacting with a cavity field as depicted in Fig. 3-1. In the dipole approximation, the Hamiltonian of the system reads

$$H = H_a + H_f - e\vec{r}\cdot\vec{E}, \tag{1.5}$$

where H_a and H_f are the free energies of the atom and the cavity field, respectively. The free Hamiltonian H_f can be written as

$$H_f = \sum_{\vec{k}} \hbar\omega_c^k (a_{\vec{k}}^\dagger a_{\vec{k}} + \frac{1}{2}), \tag{1.6}$$

where $a_{\vec{k}}$ and $a_{\vec{k}}^\dagger$ are the annihilation and the creation operators of the corresponding mode of the cavity field of frequency ω_c^k.

Now, let the states $|e\rangle$ and $|g\rangle$ be the excited and the ground states of the two-level atom, respectively. We define the atomic transition operators as

$$\sigma_{ij} = |i\rangle\langle j|,\ i,j \in \{e,g\} \tag{1.7}$$

Since $|e\rangle\langle e| + |g\rangle\langle g| = 1$ and $H_a|i\rangle = E_i|i\rangle$ with $i = e, g$, we can write

$$H_a = \sum_i E_i \sigma_{ii}, \tag{1.8}$$

$$e\vec{r} = \sum_{i,j} d_{ij}\sigma_{ij}, \tag{1.9}$$

where $d_{ij} = e\langle i|\vec{r}|j\rangle$ is the matrix element of electric-dipole operator. In the dipole approximation, the electric field operator can be written as

$$\vec{E} = \sum_{\vec{k}} \hat{\epsilon}_{\vec{k}} \Gamma_{\vec{k}} (a_{\vec{k}} + a_{\vec{k}}^\dagger), \tag{1.10}$$

where $\Gamma_{\vec{k}} = (\hbar\omega_c^k/2\epsilon_0 V)^{1/2}$ with V being the volume of the cavity. Thus, the Hamiltonian 1.5 can be written as

$$H = \sum_{\vec{k}} \hbar\omega_c^k a_{\vec{k}}^\dagger a_{\vec{k}} + \sum_i E_i \sigma_{ii} + \hbar \sum_{i,j} \sum_{\vec{k}} g_{\vec{k}}^{ij} \sigma_{ij} (a_{\vec{k}} + a_{\vec{k}}^\dagger), \tag{1.11}$$

where we define the atom-field coupling strength

$$g_{\vec{k}}^{ij} = -\frac{d_{ij}\hat{\epsilon}_{\vec{k}}\Gamma_{\vec{k}}}{\hbar}. \tag{1.12}$$

Now, let us define

$$\begin{aligned} \sigma_z &= \sigma_{ee} - \sigma_{gg}, \\ \sigma_+ &= \sigma_{eg}, \\ \sigma_- &= \sigma_{ge}, \end{aligned} \tag{1.13}$$

with $E_e - E_g = \hbar\omega_a$ and $g_{\vec{k}} = g_{\vec{k}}^{eg} = g_{\vec{k}}^{ge}$ to obtain [4]

$$H = \sum_{\vec{k}} \hbar\omega_c^k a_{\vec{k}}^\dagger a_{\vec{k}} + \frac{1}{2}\hbar\omega_a \sigma_z + \hbar \sum_{\vec{k}} g_{\vec{k}} (\sigma_+ + \sigma_-)(a_{\vec{k}} + a_{\vec{k}}^\dagger). \tag{1.14}$$

Thus, for a single mode of field interacting with a two-level atom, we obtain

$$H = \hbar\omega_c a^\dagger a + \frac{1}{2}\hbar\omega_a \sigma_z + \hbar g(\sigma_+ + \sigma_-)(a + a^\dagger). \tag{1.15}$$

This Hamiltonian is one of the most important building blocks of cavity quantum electrodynamics (cQED) and known as the Rabi model [1, 2] of light-matter interactions. Aside from some new attempts to solve the Rabi model analytically [5], the full quantum spectrum of the Hamiltonian is still not known up to the date. Hence, it is only logical to find some approximate models which follows from the Rabi model as we are going to discuss in the next section.

1.1.2 Rotating-wave approximation and the Jaynes-Cummings model

The physical processes included in the Rabi model 1.15 can be summarized as follows:

- $a\sigma_+$: one photon is absorbed and the atom is excited
- $a^\dagger\sigma_-$: one photon is emitted and the atom is de-excited
- $a^\dagger\sigma_+$: one photon is emitted and the atom is excited
- $a\sigma_-$: one photon is absorbed and the atom is de-excited

The terms $a\sigma_+$ and $a^\dagger\sigma_-$ are energy conserving and vary slowly in time for weak coupling strengths. On the other hand, the terms $a^\dagger\sigma_+$ and $a\sigma_-$ do not conserve the energy. The approximation in which the latter energy non-conserving (and rapidly oscillating) terms neglected is called the rotating-wave approximation (RWA). Hence, in RWA and dipole approximations, we obtain a Hamiltonian of the form:

$$H = \hbar\omega_c a^\dagger a + \frac{1}{2}\hbar\omega_a\sigma_z + \hbar g(\sigma_+ a + \sigma_- a^\dagger). \tag{1.16}$$

This is the celebrated Jaynes-Cummings (JC) model [3]. Unlike the full Rabi Hamiltonian, it can be solve analytically and constitutes the essence of many problems on quantum optics in the literature. The eigen-spectrum of the JC model can be found in any standard text book on quantum optics and will not be given here.

1.2 Superconducting qubits

A certain analogy can be made between the field modes of an optical cavity and the vibrational modes of a coplanar waveguide resonator (CPW) [6]. It is, then, the question of creating artificial two (or more) level systems which may simulate the real atoms and can interact with the modes of a CPW resonator. Such systems are mostly composed of Josephson junctions [7, 8] and called the superconducting qubits [6].

They can be vary depending on their coupling to a given architecture, control mechanisms and auxiliary ingredients that may be added to the specified architecture. Due to its relevance, here, we only discuss a single type of a superconducting qubit called the flux qubit. We start with a brief description of the Josephson junction [7] and finalise with the coupling of atom (spins) to the superconducting qubits.

1.2.1 The Josephson junction

A Josephson junction [7] is formed by two superconducting electrodes separated by an insulator as depicted in Fig. 3-2. The super-current across the superconducting

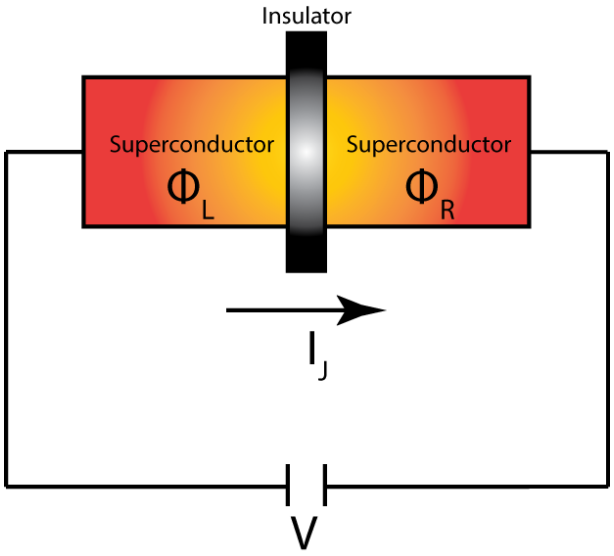

Figure 1-2: The Josephson junction.

electrodes obeys the (classical) equations of the form:

$$I_J = I_0 \sin\alpha, \tag{1.17}$$

$$V = \frac{\Phi_0}{2\pi}\frac{\partial\alpha}{\partial t}, \tag{1.18}$$

where $\Phi_0 = h/2e$ is the superconducting flux quantum and I_0 is the critical current of the junction. The superconducting phase difference and the voltage across the junction are denoted by $\alpha = \Phi_L - \Phi_R$ and V, respectively.

If the insulating barrier is thick, the electrons can not get through. But, if the insulating barrier is thin enough, electrons can tunnel through it and this phenomenon is known as the Josephson tunneling.

1.2.2 The flux qubit

Here, we discuss one of the fundamental and well known artificial qubits called the flux qubit. Let us consider a rf superconducting quantum interface device (SQUID) with a loop with one junction as depicted in Fig. 3-3. In such an architecture, persistent currents flow, while the magnetic fluxes are enclosed [8] .

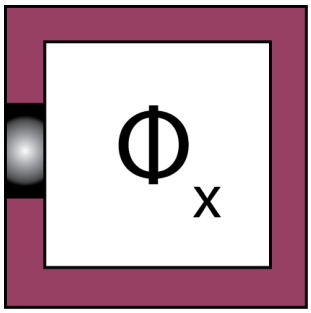

Figure 1-3: A flux qubit formed by a loop with a single junction.

The phase difference Ψ across the junction can be written in terms of the flux Φ in the loop as

$$\frac{\Psi}{2\pi} = \frac{\Phi}{\Phi_0}, \tag{1.19}$$

where Φ_0 is the flux quantum defined in the previous section. Now, if we apply an external flux Φ_x to bias the system, the Hamiltonian of the system reads [8]

$$H = -E_J \cos\left[2\pi \frac{\Phi}{\Phi_0}\right] + \frac{(\Phi - \Phi_x)^2}{2L} + \frac{Q^2}{2C_J}. \tag{1.20}$$

Here, L is the self-inductance of the loop, E_J is the Josephson energy, C_J is the capacitance of the junction and $Q = -i\hbar\partial/\partial\Phi$ is the conjugate charge.

If the self-inductance is large such that

$$\kappa_J = \frac{E_J}{(\Phi_0^2/4\pi^2 L)} > 1, \tag{1.21}$$

and the external flux Φ_x is tuned such that it is closed to $\Phi_0/2$, then the first two terms of the Hamiltonian 1.20 behave as a double well potential [8] . The Hamiltonian of the effective (two-level) model takes the form [8]

$$H = -\frac{1}{2}\left[B_z\sigma_z + B_x\sigma_x\right], \tag{1.22}$$

where B_x is the tunnelling amplitude between the wells, $B_z = 4\pi\sqrt{6(\kappa_J - 1)}E_J(\Phi_x/\Phi_0 - 1/2)$ is the bias and $\sigma_i, i = x, z$ are the Pauli matrices.

1.2.3 Interaction of atoms with superconducting qubits

Superconducting qubits can be coupled with atoms (spins) directly or indirectly [6]. In the latter, the hybrid quantum circuit is formed by a CPW resonator that is coupled with superconducting qubits and atoms, separately. Therefore, CPW resonator bears the role of intermediatery coupler between artificial qubits and atoms. The Hamiltonians of the artificial qubit-resonator and atom-resonator systems are in the form of that of two independent JC models. In the case of more than one atom coupled to the same mode of the resonator, the model is called the Tavis-Cummings model that describes the collective coupling of atoms to the same resonator (field) mode in the RWA and the dipole approximations.

Here, we are interested in hybrid systems where the superconducting qubits and atoms are directly coupled to each other via electromagnetic fields. The dynamics of a hybrid system composed of a single superconducting qubit directly coupled to a single atom can be described by the Hamiltonian of the form [6]

$$H = \hbar\omega_a\sigma_a^+\sigma_a^- + \hbar\omega_{scq}\sigma_{scq}^+\sigma_{scq}^- + \hbar g_{a-scq}(\sigma_a^-\sigma_{scq}^+ + \sigma_a^+\sigma_{scq}^-), \tag{1.23}$$

where g_{a-scq} is the coupling strength. The interaction term is active only for resonant

or near resonant systems, i.e., $|\omega_a - \omega_{scq}| \ll g_{a-scq}$, whereas it is negligible for systems that are far detuned from each other, i.e., $||\omega_a - \omega_{scq}| \gg g_{a-scq}$.

1.3 Discrete time quantum random walks

A quantum random walk is the production of the random movement of a quantum particle around a graph. Two kinds of quantum walks have considered as follows [9]:

- Continuous time quantum walks consists of a walker and a Hamiltonian operator which is applied for any times to the quantum state of the walker in the Schrödinger picture.

- Discrete time quantum walks consists of a walker and a coin both are considered as quantum mechanical systems. The composite system evolves by applying a unitary evolution operator on walker and coin states in discrete time steps.

Quantum walks is a key tool for developing quantum algorithms which are essential for universal quantum computation (see Ref. [9] and references therein). As we shall discuss in the last chapter of the present thesis, they may provide fast and secure quantum information transfer between spatially separated parties due to their property of the quadratic gain in the phase diffusion over that of a classical random walk.

1.3.1 Quantum walk on a line

Let us consider a quantum particle (the walker) whose movement is confined in one dimension. Here, the coin is represented by a qubit (or a two-level system). We can express the two levels of the qubit with the states as up $|\uparrow\rangle$ and down $|\downarrow\rangle$. Now, during each discrete step, we first apply the Hadamard operation

$$H = \frac{1}{\sqrt{2}} \begin{pmatrix} 1 & 1 \\ 1 & -1 \end{pmatrix}, \tag{1.24}$$

which transforms, e.g., the down state $|\downarrow\rangle$ to a superposition state $1/\sqrt{2}(|\uparrow\rangle + |\downarrow\rangle)$. We, then, apply an operation on the walker such that it steps left if the qubit is up and steps right if the qubit is down. The total evolution of the system can be described by a unitary operator of the form [10]

$$U_L = e^{ip\sigma_z} H, \tag{1.25}$$

where p is the momentum operator of the walker and σ_z is the Pauli spin operator which acts only on the coin. Thus, after k steps, the state of the system is given by

$$|\phi_k\rangle = (U_L)^k |\phi_0\rangle, \tag{1.26}$$

where $|\phi_0\rangle$ is the initial state of the system.

1.3.2 Quantum walk on a circle

Here, the set up almost remains the same, only change is now the walker can move in a two dimensional phase space. The algorithm of the quantum walk is the successive application of a Hadamard operation and a rotation which changes the state of the walker by an angle, say, γ [11]. The rotation is conditioned on the state of the qubit as before and the unitary evolution operator for this case reads

$$U_C = e^{i(x^2+p^2)\sigma_z \gamma} H, \tag{1.27}$$

where H is the Hadamard operator given in Eq. 1.24 and x and p are the position and momentum operators of the walker in the phase space, respectively. Thus, if the initial state of the system is $|\psi_0\rangle$, after k steps the state of the system becomes $|\psi_k\rangle = (U_C)^2 |\psi_0\rangle$.

Chapter 2

Transfer of spin squeezing and particle entanglement between atoms and photons in coupled cavities via two-photon exchange

Recent investigations of quantum tunneling dynamics of two bosonic particles in photonic [12] and atomic [13] settings reveal their rich dynamical features, not available to typical single particle tunneling situation. In the case of ultracold atoms in optical lattices, pairwise tunneling yields rich quantum phase diagrams [14]. It is proposed that two-boson tunneling can be realized by coupling molecular states to atomic ones. Similar scenario was considered before for spin squeezing [15, 16] and entanglement generation. Entanglement properties of two-photon exchange coupled cavities was analyzed in detail for the cases of two and four dimensional Hilbert space systems. These results could set the pathway towards massively correlated multiphoton nonlinear quantum optical systems [17, 18], which are rapidly developing modern subjects nowadays. The motivation of interest to such systems is their promise in quantum switching, quantum communication and computation and quantum phase transition applications.

Motivated by the link between the two-particle tunneling in atomic systems and spin squeezing, as well as its generation schemes based upon quantum state transfer between optical and atomic systems [19, 20, 21, 22, 23, 24], our aim is to investigate similar spin squeezing route to particle entanglement in two-photon exchange coupled optical cavity system. Previous studies investigate entanglement in the whole atom-photon Hilbert space in two and four dimensions [12]. Our objective is to examine spin squeezing within photon and atom subsystems and to consider possible transfer of the particle entanglement between the two subsystems.

Here, we reveal the inherit two-axis twisting spin squeezing interaction nature of two-photon exchange interaction. The non-local interaction between the cavities induces spin-squeezing in the photon subsystem. Induced spin-squeezing in the photon subsystem is then transferred to the atomic subsystem by the local atom-photon coupling within each cavity. We consider the cases of initially entangled and non-entangled photons. Spin squeezing is witnessed by the optimal spin squeezing inequalities [25].

2.1 Spin Squeezing and Particle Entanglement

Spin squeezing [26] can be defined in terms of Heisenberg uncertainty. Such a definition is subjective to choice of coordinate system. Alternative definition, that takes into account quantum correlations between individual atomic spins, is given by Kitagawa and Ueda [15] in the form

$$\xi = \frac{\Delta J_{\perp}}{\sqrt{J/2}} \tag{2.1}$$

where $J_{\perp}$ is the angular momentum component in the direction of the unit vector $\vec{n}$ along which $\Delta\vec{n}\cdot\vec{J}$ is minimized and $J/2$ is the total variance of each individual spin-1/2. If $\xi < 1$ the system is said to be spin squeezed.

Another spin squeezing criteria, which combines spin squeezing with particle en-

tanglement, is given by [16]

$$\xi_e^2 = \frac{N(\Delta J_{n_1})^2}{\langle J_{n_2}\rangle^2 + \langle J_{n_3}\rangle^2} \geq 1 \tag{2.2}$$

where N is the number of particles in the system, $J_n = \vec{n}\cdot\vec{J}$ and the $\vec{n}$s are mutually orthogonal unit vectors. The condition $\xi_e^2 < 1$ witnesses not only spin squeezing but also the particle entanglement. Particle entanglement happens in the first quantization and hence is fundamentally different than so called mode entanglement that occurs in second quantization [27, 28, 29].

On the other hand, there exist states for which spin squeezing parameter given in Ineq. 2.2 cannot be used to analyze quantum entanglement [30]. Alternatively, one may use the following inequalities since it has been shown that [25] violation of any of them implies entanglement:

$$\langle J_x^2\rangle + \langle J_y^2\rangle + \langle J_z^2\rangle \leq \frac{N(N+2)}{4} \tag{2.3a}$$

$$(\Delta J_x)^2 + (\Delta J_y)^2 + (\Delta J_z)^2 \geq \frac{N}{2} \tag{2.3b}$$

$$\langle J_k^2\rangle + \langle J_l^2\rangle - \frac{N}{2} \leq (N-1)(\Delta J_m)^2 \tag{2.3c}$$

$$(N-1)[(\Delta J_k)^2 + (\Delta J_l)^2] \geq \langle J_m^2\rangle + \frac{N(N-2)}{4} \tag{2.3d}$$

where i, j, k take all the possible permutations of x, y, z. These inequalities are called optimal spin squeezing inequalities. The Ineq. 2.3c is equivalent to the Ineq. 2.2 for a system of many particles which has a maximal spin in some direction [31] and they can be related to the positivity of concurrence [32]. Very recently, these inequalities generalized for qudits with arbitrary spin [33].

Entanglement is considered as quantum information resource, and hence it is desirable to be able transfer entanglement between distant nodes in a quantum network [19, 20]. In the following section we shall review the two-photon hopping model and argue that it can serve as an efficient tool for establishing particle entanglement between distant atoms via transfer of entanglement from photon subsystem to atom

subsystem.

2.2 The Model

We consider a system of two spatially separated optical cavities, each containing a single atom, that is interacting with the cavity field by two-photon transitions. The cavities are coupled to each other with two-photon exchange. The Hamiltonian of the system is written by [12, 34, 35, 36]

$$H = H^{(1)} - H_0^{(1)} + H^{(2)} - H_0^{(2)} + \hbar\zeta(a_1^{\dagger 2}a_2^2 + a_2^{\dagger 2}a_1^2), \tag{2.4}$$

where

$$\begin{aligned} H^{(i)} &= \hbar\omega a_i^\dagger a_i + \hbar\omega(\sigma_{ee}^{(i)} - \sigma_{gg}^{(i)}) + \hbar\mu\sigma_{ee}^{(i)} \\ &+ \hbar\eta\sigma_{gg}^{(i)} + \hbar\lambda(\sigma_{eg}^{(i)}a_i^2 + \sigma_{ge}^{(i)}a_i^{\dagger 2}), \end{aligned} \tag{2.5}$$

and

$$H_0^{(i)} = \hbar\omega(a_i^\dagger a_i + \sigma_{ee}^{(i)}) - \sigma_{gg}^{(i)} + (E_g + E_e)/2, \tag{2.6}$$

with E_g, E_e being the energies of the ground and exited states, respectively. The last term in the Eq. 3.1 is the two-photon exchange interaction between the cavities, characterized by the hopping rate ζ. The parameters μ, η and λ are the free energies of the subsystems and the two-photon transition rate written in the convention of Ref. [37], $\sigma_{kl}^{(i)} = |k\rangle^{(i)(i)}\langle l|$ are the atomic transition operators, k and l denotes either ground (g) or exited (e) states of the atom and $i = 1, 2$ labels the cavities. Here, the hopping rate ζ, time t and the eigenfrequencies ω_is will be scaled by the free energy λ in numerical calculations. Therefore, in all figures where $\zeta \leq 1$ corresponds to the local interaction dominant regimes, while $\zeta > 1$ corresponds to the hopping dominant regimes.

The spin components for a system of two level atoms defined by [23]

$$\begin{aligned} S_x &= \frac{1}{2}(\sigma_{eg} + \sigma_{ge}) \\ S_y &= \frac{-i}{2}(\sigma_{eg} - \sigma_{ge}) \\ S_z &= \frac{1}{2}(\sigma_{ee} - \sigma_{gg}). \end{aligned} \tag{2.7}$$

Since we are interested in two coupled cavities each has one atom, we define the spin components of the atoms for this configuration as follows

$$\begin{aligned} S_x &= S_x^{(1)} \otimes 1^{(2)} + 1^{(1)} \otimes S_x^{(2)} \\ S_y &= S_y^{(1)} \otimes 1^{(2)} + 1^{(1)} \otimes S_y^{(2)} \\ S_z &= S_z^{(1)} \otimes 1^{(2)} + 1^{(1)} \otimes S_z^{(2)} \end{aligned} \tag{2.8}$$

where the superscripts (1) and (2) are label the first and second cavities, respectively.

Likewise, we can consider pseudo-spin operators for the coupled cavity field such that

$$\begin{aligned} L_x &\equiv \frac{1}{2}(a_1^\dagger a_2 + a_2^\dagger a_1), \\ L_y &\equiv \frac{-i}{2}(a_1^\dagger a_2 - a_2^\dagger a_1), \\ L_z &\equiv \frac{1}{2}(a_1^\dagger a_1 - a_2^\dagger a_2). \end{aligned} \tag{2.9}$$

They satisfy the SU(2) spin algebra $[L_\alpha, L_\beta] = \epsilon^{\alpha\beta\gamma} L_\gamma$. Here $\alpha, \beta, \gamma \in \{x, y, z\}$ and $\epsilon^{\alpha\beta\gamma}$ is the Levi-Civita density. In terms of $L_+ \equiv L_x + iL_y = a_1^\dagger a_2$ and $L_- \equiv L_x - iL_y = a_2^\dagger a_1$, it is straightforward to rewrite two-photon hopping interaction Hamiltonian $H_p = \hbar\zeta(a_1^{\dagger 2} a_2^2 + a_2^{\dagger 2} a_1^2)$ as

$$H_p = \hbar\zeta(L_+^2 + L_-^2) = 2\hbar\zeta(L_x^2 - L_y^2). \tag{2.10}$$

This is nothing but the two-axis twisting Hamiltonian which squeezes the spin states by twisting them about the two axes [15]. Clearly neither spin squeezing nor associ-

ated particle entanglement can be achieved via one photon hopping in coupled-cavity systems, as the coupling term would be a mere rotation operation generated by L_x, though it would produce mode entanglement.

It should be noted that in collective spin systems, i.e., systems in which all spins mutually interact, Eq. 2.10 is known as the Lipkin-Meshkov-Glick (LMG) Hamiltonian whose entanglement dynamics and exact properties in the thermodynamical limit have been carefully analyzed in Ref. [38, 39, 40]. Alternatively, the two-photon hopping can also be seen as a special case of more general nonlinear quantum optical Karassiov-Klimov models [41]. Following the Lie-algebraic approach, two-photon hopping term can be recognized by a Jordan-Schwinger map as the difference of raising and lowering operators of the Higgs algebra [42]. In the view of background field method in the Fokker-Plank formalism [43], we then expect that fluctuations of (Higgs or deformed) effective photon spin operators drive fluctuations of collective atomic spin operators coupled to two-photon transition operators. Fluctuations of two- photon transition operators can be further linked to the quadrature variances. We would then intuitively expect that reduction of spin noise from photon subsystem could be transferred to the atomic subsystem through reduction of quadrature noise. We shall numerically investigate these intuitive expectations for some initial cases in the following section.

2.3 Squeezing and Entanglement Transfer

In this section we investigate the transfer of spin squeezing and particle entanglement between distant cavities. To do that, we shall obtain the optimal spin squeezing inequalities for the atomic and photonic systems separately, analyze their variations in time and compare them with each other.

For a given initial state $|\psi(0)\rangle$, restricted to two-photon manifold, the time-

dependent state vector $|\psi(t)\rangle$ may be written as

$$\begin{aligned} |\psi(t)\rangle &= A(t)|g,2\rangle^1|g,0\rangle^2 + B(t)|g,0\rangle^1|g,2\rangle^2 \\ &+ C(t)|g,0\rangle^1|e,0\rangle^2 + D(t)|e,0\rangle^1|g,0\rangle^2. \end{aligned} \tag{2.11}$$

The general solution of the time-dependent Schrödinger equation $i\hbar\partial_t|\psi(t)\rangle = H|\psi(t)\rangle$ in the two-dimensional submanifold of the Hilbert space is [12]

$$\begin{aligned} |\psi(t)\rangle &= (A_1 e^{-i\omega_1 t} + A_2 e^{-i\omega_2 t})|\phi_1\rangle + (A_3 e^{-i\omega_3 t} + A_4 \\ &\quad e^{-i\omega_4 t})|\phi_2\rangle + (\alpha_1 A_1 e^{-i\omega_1 t} + \alpha_2 A_2 e^{-i\omega_2 t})|\phi_3\rangle \\ &\quad (\alpha_3 A_3 e^{-i\omega_3 t} + \alpha_4 A_4 e^{-i\omega_4 t})|\phi_4\rangle \end{aligned} \tag{2.12}$$

where $\alpha_i = \sqrt{2}/2(\omega_i - 0.5)$, ω_is are the eigenfrequencies described explicitly in [12] as well as A_is and

$$|\phi_1\rangle = \frac{1}{\sqrt{2}}(|g,2\rangle^1|g,0\rangle^2 + |g,0\rangle^1|g,2\rangle^2) \tag{2.13a}$$

$$|\phi_2\rangle = \frac{1}{\sqrt{2}}(|g,2\rangle^1|g,0\rangle^2 - |g,0\rangle^1|g,2\rangle^2) \tag{2.13b}$$

$$|\phi_3\rangle = \frac{1}{\sqrt{2}}(|e,0\rangle^1|g,0\rangle^2 + |g,0\rangle^1|e,0\rangle^2) \tag{2.13c}$$

$$|\phi_4\rangle = \frac{1}{\sqrt{2}}(|e,0\rangle^1|g,0\rangle^2 - |g,0\rangle^1|e,0\rangle^2). \tag{2.13d}$$

The states in Eq. 2.13 are mutually orthogonal and entangled. Since, this solution allows for Rabi oscillations, one can transfer entanglement between the symmetric ($|\phi_1\rangle$ and $|\phi_3\rangle$) and antisymmetric ($|\phi_2\rangle$ and $|\phi_4\rangle$) states separately [12].

2.3.1 Initially Entangled Photons

Let us first start with a state which is initially entangled

$$|\psi(0)\rangle = \frac{1}{\sqrt{2}}(|g,2\rangle^1|g,0\rangle^2 + |g,0\rangle^1|g,2\rangle^2). \tag{2.14}$$

Then, at time t, we have

$$\begin{aligned} |\psi(t)\rangle &= A_1(e^{-i\omega_1 t} + \alpha_1^2 e^{-i\omega_2 t})|\phi_1\rangle \\ &+ \alpha_1 A_1(e^{-i\omega_1 t} - e^{-i\omega_2 t})|\phi_3\rangle \end{aligned} \tag{2.15}$$

with $A_1 + \alpha_1^2 A_1 = 1$. For atom-photon system the density operator, $\rho_{ap}^{12}(t)$, becomes

$$\begin{aligned} \rho_{ap}^{12}(t) &= |A|^2|\phi_1\rangle\langle\phi_1| + AB^*|\phi_1\rangle\langle\phi_3| \\ &+ BA^*|\phi_3\rangle\langle\phi_1| + |B|^2|\phi_3\rangle\langle\phi_3| \end{aligned} \tag{2.16}$$

where

$$|A|^2 = A_1^2[1 + 2\alpha_1^2\cos(\delta_{12}t) + \alpha_1^4] \tag{2.17a}$$

$$AB^* = \alpha_1 A_1^2[1 - \alpha_1^2 + \alpha_1^2 e^{i\delta_{12}t} - e^{-i\delta_{12}t}] \tag{2.17b}$$

$$|B|^2 = 2\alpha_1^2 A_1^2[1 - \cos(\delta_{12}t)] \tag{2.17c}$$

and $\delta_{12} = \omega_1 - \omega_2$. To obtain reduced density operators $\rho_a^{12}(t)$ and $\rho_p^{12}(t)$ for atomic and photonic systems respectively we take partial traces as

$$\begin{aligned} \rho_a^{12}(t) &= Tr_p\rho_{ap}^{12}(t) = |A|^2|g\rangle^{11}\langle g| \otimes |g\rangle^{22}\langle g| \\ &+ \frac{|B|^2}{2}(|e\rangle^{11}\langle e| \otimes |g\rangle^{22}\langle g| + |e\rangle^{11}\langle g| \otimes |g\rangle^{22}\langle e| \\ &+ |g\rangle^{11}\langle e| \otimes |e\rangle^{22}\langle g| + |g\rangle^{11}\langle g| \otimes |e\rangle^{22}\langle e|) \end{aligned} \tag{2.18}$$

and

$$\begin{aligned} \rho_p^{12}(t) &= Tr_a\rho_{ap}^{12}(t) = \frac{|A|^2}{2}(|2,0\rangle\langle 2,0| + |2,0\rangle\langle 0,2| \\ &+ |0,2\rangle\langle 2,0| + |0,2\rangle\langle 0,2|) + |B|^2|0,0\rangle\langle 0,0|. \end{aligned} \tag{2.19}$$

Ineq. 2.3d gives the following inequalities for atomic and photonic subsystems, respectively:

$$Ineq_a \equiv 4 - 5|A|^2 \leq 0, \tag{2.20}$$

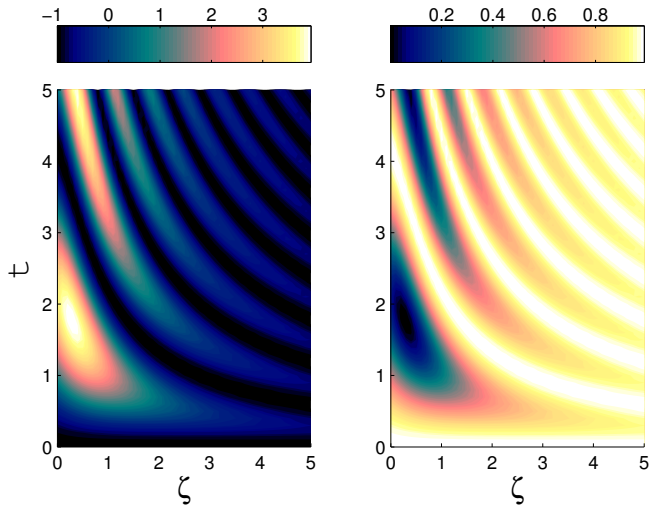

Figure 2-1: Variation of spin squeezing in atomic (left) and photonic (right) subsystems, with respect to time and hopping constant. ζ is scaled by λ and $\zeta \leq 1$ corresponds to the local interaction dominant regimes, while $\zeta > 1$ corresponds to the hopping dominant regimes. Spin squeezing is characterized positive values in both figures. At $t = 0$, $Ineq_a = -1$ and $Ineq_p = 1$. All the parameters plotted are dimensionless as explained in the text.

$$Ineq_p \equiv |A|^2 \leq 0, \tag{2.21}$$

where we take $k = x$, $l = z$, $m = y$ in Ineq. 2.20 and $k = z, l = y$ and $m = x$ in Ineq. 2.21. Violation of these inequalities imply spin squeezing (and particle entanglement) in the corresponding systems and as it can be easily seen from the Fig.3-1, indeed this is the case. Initially we have non-entangled atoms and entangled photons. As time goes on, atomic system becomes entangled which induced by the photons, i.e., we have entanglement and spin squeezing transfer. Transfers occur periodically in the local-interaction regime ($\zeta < 1$). In the hopping dominant regime, atoms are not entangled or spin squeezed, while the photons are. As should be expected, almost pure two-photon entanglement regimes occur more frequent and in broader intervals with the increase of two-photon hopping rate.

2.3.2 Initially Non-Entangled State

We next consider initially a non-entangled state of the form

$$|\psi(0)\rangle = |g,2\rangle^1|g,0\rangle^2 \tag{2.22}$$

which evolves in time as

$$\begin{aligned} |\psi(t)\rangle &= A_1(e^{-i\omega_1 t} + \alpha_1^2 e^{-i\omega_2 t})|\phi_1\rangle \\ &+ \alpha_1 A_1(e^{-i\omega_1 t} - e^{-i\omega_2 t})|\phi_3\rangle \\ &+ A_3(e^{-i\omega_3 t} + \alpha_3^2 e^{-i\omega_4 t})|\phi_2\rangle \\ &+ \alpha_3 A_3(e^{-i\omega_3 t} - e^{-i\omega_4 t})|\phi_4\rangle. \end{aligned} \tag{2.23}$$

The density operator, ρ_{ap}^{12}, for this case then reads

$$\begin{aligned} \rho_{ap}^{12}(t) &= |A|^2|\phi_1\rangle\langle\phi_1| + AB^*|\phi_1\rangle\langle\phi_3| + AC^*|\phi_1\rangle\langle\phi_2| + AD^*|\phi_1\rangle\langle\phi_4| \\ &+ BA^*|\phi_3\rangle\langle\phi_1| + |B|^2|\phi_3\rangle\langle\phi_3| + BC^*|\phi_3\rangle\langle\phi_2| + BD^*|\phi_3\rangle\langle\phi_4| \\ &+ CA^*|\phi_2\rangle\langle\phi_1| + CB^*|\phi_2\rangle\langle\phi_3| + |C|^2|\phi_2\rangle\langle\phi_2| + CD^*|\phi_2\rangle\langle\phi_4| \\ &+ DA^*|\phi_4\rangle\langle\phi_1| + DB^*|\phi_4\rangle\langle\phi_3| + DC^*|\phi_4\rangle\langle\phi_2| + |D|^2|\phi_4\rangle\langle\phi_4| \end{aligned} \tag{2.24}$$

where

$$AC^* = A_1A_3[e^{i(\omega_3-\omega_1)t} + \alpha_3^2 e^{i(\omega_4-\omega_1)t} + \alpha_1^2 e^{i(\omega_3-\omega_2)t} + \alpha_1^2\alpha_3^2 e^{i(\omega_4-\omega_2)t}] \tag{2.25a}$$

$$AD^* = \alpha_3 A_1A_3[e^{i(\omega_3-\omega_1)t} - e^{i(\omega_4-\omega_1)t} + \alpha_1^2(e^{i(\omega_3-\omega_2)t} - e^{i(\omega_4-\omega_2)t})] \tag{2.25b}$$

$$BC^* = \alpha_1 A_1A_3[e^{i(\omega_3-\omega_1)t} - e^{i(\omega_3-\omega_2)t} + \alpha_3^2(e^{i(\omega_4-\omega_1)t} - e^{i(\omega_4-\omega_3)t})] \tag{2.25c}$$

$$BD^* = \alpha_1\alpha_3 A_1A_3[e^{i(\omega_3-\omega_1)t} + e^{i(\omega_4-\omega_2)t} - e^{i(\omega_4-\omega_1)t} - e^{i(\omega_3-\omega_2)t}] \tag{2.25d}$$

$$CD^* = \alpha_3 A_3^2[1 - e^{i(\omega_4-\omega_3)t} + \alpha_3^2(e^{i(\omega_3-\omega_4)t} - 1)] \tag{2.25e}$$

$$|C|^2 = A_3^2[1 + 2\alpha_3^2\cos[(\omega_3-\omega_4)t] + \alpha_3^4] \tag{2.25f}$$

$$|D|^2 = 2\alpha_3^2 A_3^2[1 - \cos[(\omega_3-\omega_4)t]] \tag{2.25g}$$

with $A_1(1+\alpha_1^2) = A_3(1+\alpha_3^2) = 1/\sqrt{2}$ and $|A|^2$, $|B|^2$, AB^* are given in Eq. 2.17. The reduced density operators are given by

$$\begin{aligned}\rho_a^{12}(t) &= (|A|^2+|C|^2)|g\rangle^{11}\langle g|\otimes|g\rangle^{22}\langle g| + \frac{1}{2}\big[(|B|^2+|D|^2+BD^* \\ &+ DB^*)|e\rangle^{11}\langle e|\otimes|g\rangle^{22}\langle g| + (|B|^2-|D|^2-BD^*+DB^*)|e\rangle^{11}\langle g|\otimes|g\rangle^{22}\langle e| \\ &+ (|B|^2-|D|^2+BD^*-DB^*)|g\rangle^{11}\langle e|\otimes|e\rangle^{22}\langle g| \\ &+ (|B|^2+|D|^2-BD^*-DB^*)|g\rangle^{11}\langle g|\otimes|e\rangle^{22}\langle e|\big] \qquad (2.26)\end{aligned}$$

$$\begin{aligned}\rho_p^{12}(t) &= \frac{1}{2}\big[(|A|^2+AC^*+CA^*)|2,0\rangle\langle 2,0| + (|A|^2-AC^*+CA^*)|2,0\rangle\langle 0,2| \\ &+ (|A|^2+AC^*-CA^*)|0,2\rangle\langle 2,0| + (|A|^2-AC^*-CA^*)|0,2\rangle\langle 0,2|\big] \\ &+ (2|B|^2+|D|^2)|0,0\rangle\langle 0,0|. \qquad (2.27)\end{aligned}$$

Then, Ineq. 2.3d gives

$$Ineq_a \equiv 3|B|^2 - |D|^2 - 2(|B|^2+|D|^2)^2 \geq 0, \qquad (2.28)$$

for atomic system and Ineq. 2.3b gives

$$Ineq_p \equiv 2|A|^2 - 1 \geq 0, \qquad (2.29)$$

for photonic system, where we take $k = x$, $l = z$ and $m = y$. As in the initially entangled case, violation of these inequalities imply spin squeezing (and particle entanglement) in the corresponding systems. Fig.3-2 shows that initially unentangled photons quickly get entangled and this is transferred to the atomic subsystem similar to Fig. 3-1. The Fig. 3-2 verifies the periodical nature of the transfers, by anchoring a hopping constant and observing the time evolutions. In terms of particle entanglement, then atomic system becomes more correlated at the expense of the correlation of the field particles and vice versa.

Dynamics of correlations can be further interpreted by investigating the quadra-

tures of the photonic subsystems. Local interaction of the photon-atom subsystems are of two-photon transition types and thus we expect quadrature correlations directly influence the atomic spin noise.

The quadrature operators for the field are defined as

$$X_1 = \frac{1}{2}(a^\dagger + a), \tag{2.30a}$$

$$X_2 = \frac{i}{2}(a^\dagger - a). \tag{2.30b}$$

Using the reduced density operators acting on the photonic subsystems, it can be readily shown that:

$$(\Delta X_1)^2 = (\Delta X_2)^2 = \frac{1}{4} + \frac{1}{2}|A|^2, \tag{2.31a}$$

$$(\Delta X_1)^2 = (\Delta X_2)^2 = \frac{7}{8}|A|^2 + \frac{1}{4}(AC^* + CA^* + |D|^2) + \frac{1}{2}|B|^2, \tag{2.31b}$$

for initially entangled and initially non-entangled states respectively. As we see from the Fig.3-3, for initially entangled state (left) we have ideally squeezed states at darker regions where the product of the variances of the quadratures is equal to 0.25 (since $(\Delta X_1)^2 = (\Delta X_2)^2$). The behaviour of the quadratures is very similar to that of spin squeezing inequalities for initially entangled field (see Fig.3-1).

In the case that the state is initially non-entangled, situation is even more revealing. We see from the Fig. 3-3 (right) that initially there is no quadrature squeezing. But at later times we observe such correlations; especially at the darker regions we have $(\Delta X_1)^2 = (\Delta X_2)^2 \leq 1/4$. Thus, in the light of above observations about quadratures, we conclude that (i) photon subsystem corresponds to effectively a spin system that is, under two-axis twisting interaction, squeezed, and particle entangled (ii) atoms do not directly interact with this effective spin system, but couple to the field by two-photon transitions that can be linked to quadrature squeezing. (iii) Sharing the quadrature squeezed particle entangled photons, the atoms build up sufficient

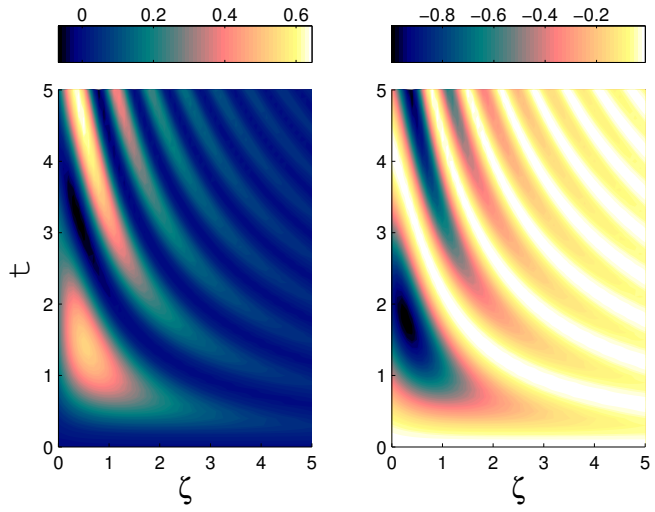

Figure 2-2: Variations of the spin squeezing in atomic (left) and photonic (right) subsystems with respect to time and hopping constant. Both inequalities are violated, therefore we have both spin squeezed and entangled systems. Spin squeezing is characterized negative values in both figures. At $t = 0$, both inequalities are equal to zero. All the parameters plotted are dimensionless as explained in the text.

noise reduction in particular directions to become spin squeezed and hence get particle entangled.

2.3.3 Physical Implementation

In Fig. 3-4, we illustrate a general scheme of possible realizations of the model [12, 37, 44]. The scheme depicts two identical coupled resonators, with cavity mode frequecies ω. Each resonator contains a three-level atom that interacts with the cavity mode in cascade formation. The detuning is given by $\Delta = E_1 - E_2 + \hbar\omega = E_3 - E_2 - \hbar\omega$ where $E_{1,2,3}$ are the energies of the corresponding levels of the atoms [37]. One of the three-levels, the state $|2\rangle$, is eliminated via a unitary transformation [12, 34, 35, 36]. The quantum states $|1\rangle$ and $|3\rangle$ correspond respectively to the $|g\rangle$ and $|e\rangle$ we have used in the earlier sections in the text. The cavities are coupled via a Kerr-type nonlinear dielectric medium that allows for two-photon interactions. It is proposed that this scheme can be implemented with superconducting circuit QED technology [44]. The proposal is based upon an extension of single photon

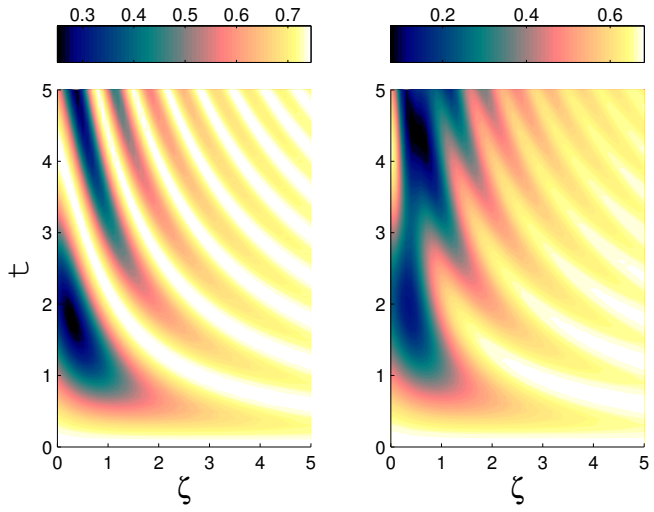

Figure 2-3: Variation of the variances of the quadratures for (left) initially entangled state and (right) initially non-entangled state with respect to time and hopping constant. Quadratures are squeezed for values ≤ 0.25. At $t = 0$, $(\Delta X_1)^2 = (\Delta X_2)^2 = 0.75$ for initially entangled state and $(\Delta X_1)^2 = (\Delta X_2)^2 = 0.6875$ for initially non-entangled state. All the parameters plotted are dimensionless as explained in the text.

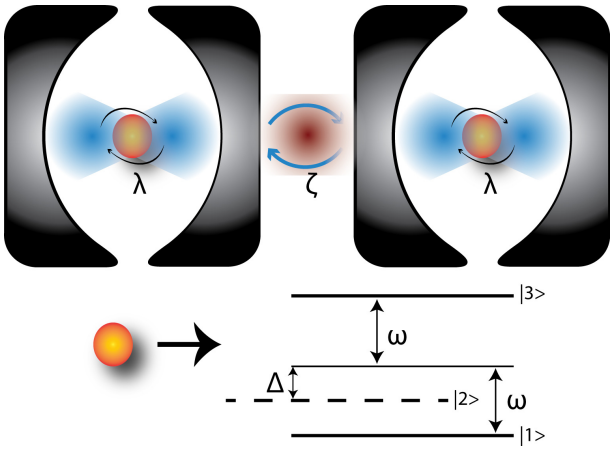

Figure 2-4: Two identical cavities, with cavity frequecies ω, coupled via two-photon exchange which is governed by a nonlinear Kerr medium. Each cavity contains a three level atom in cascade formation.

scattering and hopping in a system of two coupled superconducting transmission line resonators (TLRs). Two-photon hopping is suggested to be realized by using a nonlinear intermediate medium to couple the resonators [44]. The nonlinear dielectric

causes Kerr-type interactions [18] among the TLR photons. It is further proposed that [12] effective two-level system with two-photon transitions coupled to the resonators can be realized by using transmon qubits coupled to the resonators at their microwave field antinodes [45]. Circuit QED architectures with multi-level solid-state qubits are considered as promising systems to perform quantum information transfer operations [46]. Quantum state transfer in similar set ups, but without two-photon hopping, in circuit QED has experimentally demonstrated [47].

The model parameters μ, η and λ are all in the order of the qubit-resonator coupling as can be seen from their expressions given in the appendix. λ determines the time and energy scale that are used in reporting our results. The critical condition to observe the reported transfer of spin squeezing is then to make sure the qubit-resonator coupling is sufficiently strong relative to the decoherence rate due to solid state qubit dephasing and cavity losses. This seems to be plausible considering the recent progress towards ultrastrong coupling [48] and deep strong coupling [49] regimes of circuit QED. The hopping rate ζ is used in the text as a control parameter in our calculations, so that we present our results in terms of the relative strength of g and ζ. In other words spin squeezing is discussed as a function of relative strength of local on cavity interaction of the qubit with respect to non-local inter-cavity coupling.

The initial states considered in the text can be realized within such circuit QED set ups, similar to that in Ref. [50], where the authors have proposed a system, composed of a superconducting phase qubit coupled to a microwave resonator, that may be used for the controlled generation of multi-photon Fock states. Finally the observation of the squeezing can be performed by using similar methods developed for second order correlation function measurement [51].

2.4 Appendix

We give expressions for the parameters μ, η and λ which respectively specify the effective free energies of the subsystems and the effective two-photon transition rate in an effective two-level system. They are generated by a unitary transformation

method applied to a three-level atom in cascade formation [37]. Such a relation adds the model Hamiltonian, given in Eqn. 3.1, intensity-dependent Stark-shift terms [37] so that they are depending on the photon number through the parameter N defined below. Following the convention of the Ref. [37], these parameters are given by:

$$\hbar\lambda = \frac{g_{12}g_{23}\{[\Delta^2 + 4\hbar^2(\tilde{g}_{12}^2 + \tilde{g}_{23}^2)]^{1/2} - \Delta\}}{2(\tilde{g}_{12}^2 + \tilde{g}_{23}^2)}, \tag{2.32a}$$

$$\hbar\mu = \frac{\Delta\tilde{g}_{12}^2}{2(\tilde{g}_{12}^2 + \tilde{g}_{23}^2)} + \frac{(\tilde{g}_{12}^2 + 2\tilde{g}_{23}^2)[\Delta^2 + 4\hbar^2(\tilde{g}_{12}^2 + \tilde{g}_{23}^2)]^{1/2}}{2(\tilde{g}_{12}^2 + \tilde{g}_{23}^2)}, \tag{2.32b}$$

$$\hbar\eta = \frac{\Delta\tilde{g}_{23}^2}{2(\tilde{g}_{12}^2 + \tilde{g}_{23}^2)} + \frac{(2\tilde{g}_{12}^2 + \tilde{g}_{23}^2)[\Delta^2 + 4\hbar^2(\tilde{g}_{12}^2 + \tilde{g}_{23}^2)]^{1/2}}{2(\tilde{g}_{12}^2 + \tilde{g}_{23}^2)}, \tag{2.32c}$$

where g_{12} and g_{23} are the coupling constants for the cavity and the corresponding transitions of the atomic levels (see Fig. 3-4), $\tilde{g}_{12}^2 = g_{12}^2 N$, $\tilde{g}_{23}^2 = g_{23}^2(N-1)$ with $N = \langle a^\dagger a\rangle + \langle\sigma_{33}\rangle - \langle\sigma_{11}\rangle + 1$ is a constant of motion [12, 37] and Δ is the detuning. Here, for the clearity of equations, we did not label the parameters to distinguish cavities since they are taken to be identical.

Chapter 3

Spin squeezing, entanglement and coherence in two driven, dissipative, nonlinear cavities coupled with single and two-photon exchange

Multiphoton processes in quantum optical systems have been intensely studied [17, 18] due to their central role in modern applications such as quantum switching [52], quantum communication and computation [53]. They are also used for fundamental explorations of phase transitions in coupled nonlinear cavity or superconducting (SC) circuit quantum electrodynamics (QED) systems [54, 55, 56, 57, 58, 59, 60, 61, 62, 63, 64, 65, 66, 67, 68].

An earlier study of two nonlinear cavities coupled with single-photon exchange [69] revealed a curious interplay between coherence and localization of the photons. It is concluded that photons are coherent and delocalized over the cavities when the tunneling exchange is stronger than the nonlinearity. In the opposite case of weaker tunneling, photons are localized in each cavity and antibunched [70] .

In this chapter, we address the question if such an interplay can go across to quantum correlations as well. We specifically ask how such mutual influences between

localization, coherence and quantum entanglement [71] change under two-photon exchange [72, 73, 74] as well as under strong drive conditions [75, 76]. Realization of two-photon exchange coupling was proposed for circuit QED systems [44, 77, 78, 79, 80, 81].

Profound relations between different definitions of spin squeezing and entanglement have already been explored in detail [26, 82, 83, 84, 85]. Using Lipkin-Meshkov-Glick (LMG) Model [86], interplay of quantum correlations in squeezing and entanglement in finite quantum systems was discussed quite recently [82]. Entanglement dynamics and exact properties of LMG model in the thermodynamical limit have been carefully analyzed in Refs. [38, 39, 40]. Two photon exchange coupled cavities can also be described by the LMG model [73].

We calculate and compare the zero time delay second order quantum coherence function [4], an optimal spin squeezing inequality associated with particle entanglement [25], l-concurrence [87], genuine mode entanglement parameters [88, 89] and the von Neumann entanglement entropy [53]. Mode entanglement occurs in the second quantization description of the system; and hence it is fundamentally different from the particle entanglement, which happens in the first quantization description [27, 90, 29]. Some possible realizations and experiments to detect multiparticle entanglement via optimal spin squeezing inequalities can be found in Refs. [91, 92, 93].

Motivation for our purpose is to comprehend the relation between coherence and distinct quantum correlations and use this relation as a guide to develop viable strategies for practical realization of quantum entanglement in networks of coupled nonlinear cavities [94, 95]. These networks share characteristic models identical with ultracold atoms in optical lattices [96, 97, 98, 99, 100, 101] and quantum phase transitions of light [67] exhibit similar properties to those atomic systems [102]. Novel behaviors could emerge under strong drive and with strong local and nonlocal nonlinearities in optical systems. Distinct entanglement types under nonlocal nonlinearities and strong drive conditions and their relation to coherence are not discussed with sufficient detail in the literature. Filling these gaps could be significant for practical realization of distinct quantum entanglements in photonic cavity networks for differ-

ent simulations and applications, as well as for illuminating novel quantum phases in such systems.

3.1 The Model System

We consider a system of two identical nonlinear cavities, labeled with $i = 1, 2$, coupled either by single or two photon exchange interactions. Both cavities are driven by a coherent pump at rate F at the laser frequency ω_L. The corresponding model Hamiltonians in a frame rotating at ω_L can be written as

$$\begin{aligned} \hat{H}^{(1)} &= \sum_{i=1,2} (U\hat{b}_i^\dagger \hat{b}_i^\dagger \hat{b}_i \hat{b}_i + F\hat{b}_i^\dagger + F^*\hat{b}_i) \\ &+ J(\hat{b}_1^\dagger \hat{b}_2 + \hat{b}_2^\dagger \hat{b}_1), \end{aligned} \tag{3.1}$$

$$\begin{aligned} \hat{H}^{(2)} &= \sum_{i=1,2} (U\hat{b}_i^\dagger \hat{b}_i^\dagger \hat{b}_i \hat{b}_i + F\hat{b}_i^\dagger + F^*\hat{b}_i) \\ &+ J(\hat{b}_1^{2\dagger} \hat{b}_2^2 + \hat{b}_2^{2\dagger} \hat{b}_1^2), \end{aligned} \tag{3.2}$$

where U is the nonlinearity parameter and J is the photon exchange coefficient. Here we denote the model with single and two photon exchange coupling as $\hat{H}^{(1)}$ and $\hat{H}^{(2)}$, respectively. These models describe generic two-site Kerr-Hubbard type interactions that may be realized in settings other than coupled cavities, for example in ultracold atoms [96, 97, 98, 99, 100]. Two photon exchange term appears in dipolar spinor Bose-Einstein condensates as well [101]. Annihilation (creation) operator for the cavity photons with frequency ω_i is denoted by $\hat{b}_i$ ($\hat{b}_i^\dagger$). We take $\omega_i = \omega_L$. Transformation of the Hamiltonians to the frame rotating at ω_L removes the explicit time dependence of the drive terms and cancels the $\omega_i b_i^\dagger b_i$ terms.

Let us re-express the model Hamiltonians using the pseudo-spin operators of the

cavity fields,

$$\begin{aligned}\hat{J}_x &\equiv \frac{1}{2}(\hat{b}_1^\dagger \hat{b}_2 + \hat{b}_2^\dagger \hat{b}_1),\\ \hat{J}_y &\equiv \frac{-i}{2}(\hat{b}_1^\dagger \hat{b}_2 - \hat{b}_2^\dagger \hat{b}_1),\\ \hat{J}_z &\equiv \frac{1}{2}(\hat{b}_1^\dagger \hat{b}_1 - \hat{b}_2^\dagger \hat{b}_2).\end{aligned} \tag{3.3}$$

They satisfy the SU(2) spin algebra $[\hat{J}_\alpha, \hat{J}_\beta] = \epsilon^{\alpha\beta\gamma}\hat{J}_\gamma$. Here $\alpha, \beta, \gamma \in \{x, y, z\}$ and $\epsilon^{\alpha\beta\gamma}$ is the Levi-Civita density. We obtain

$$\hat{H}^{(1)} = U\hat{J}_z^2 + 2J\hat{J}_x + \sum_{i=1,2}(F\hat{b}_i^\dagger + F^*\hat{b}_i), \tag{3.4}$$

$$\hat{H}^{(2)} = U\hat{J}_z^2 + 2J(\hat{J}_x^2 - \hat{J}_y^2) + \sum_{i=1,2}(F\hat{b}_i^\dagger + F^*\hat{b}_i). \tag{3.5}$$

While the tunneling term is a mere rotation operator in the case of single photon exchange, it is a generator of spin squeezing that redistributes the spin fluctuations by twisting them about the two axis [15] in the case of two photon exchange. The nonlinear term always acts as a generator of spin squeezing by twisting the fluctuations around a single (z) axis. Spin squeezing is associated with multi-particle entanglement. Another type of entanglement can be found between the cavity modes. This mode entanglement is enforced by the mode coupling character of the tunneling terms. Drive term brings coherence into the system.

In the next section we define the measures of quantum correlations to calculate spin squeezing, entanglement and coherence properties of these models. All the measures are closely related to the spin noise and hence strong interplay between coherence, squeezing and types of entanglement is expected.

3.2 Results and Discussions

To investigate the quantum dynamics of our model systems under dissipation, we assume that the coupling of the cavity photons and the reservoir photons is weak;

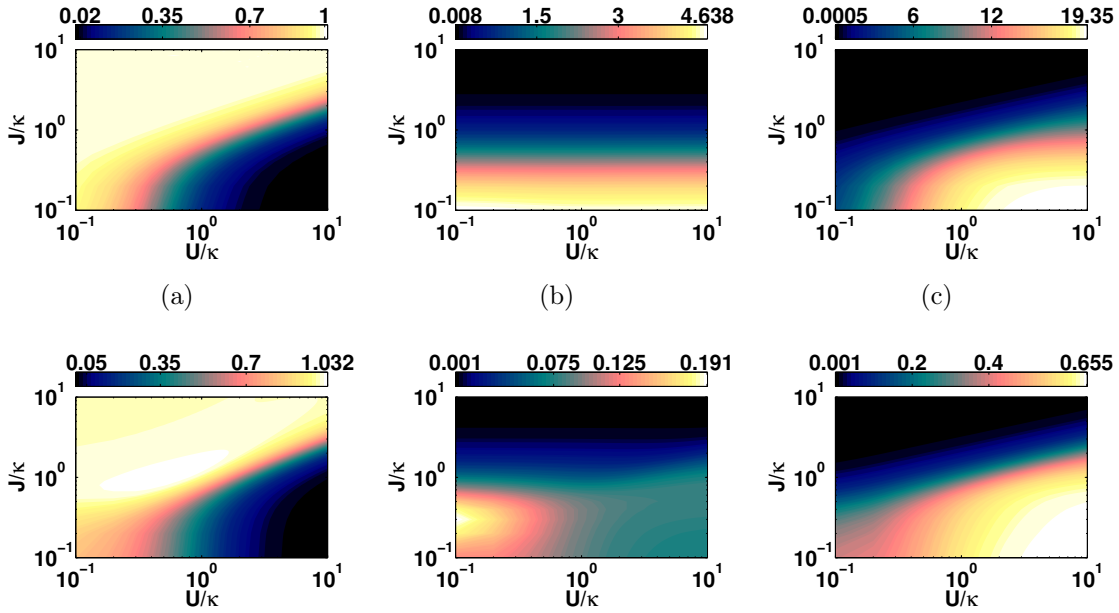

Figure 3-1: Dependence of (a) $g^{(2)}(0)$, (b) ζ (c) C_I for $F/\kappa = 0.1$ and (d) $g^{(2)}(0)$, (e) ζ (f) C_I for $F/\kappa = 1$ with respect to dimensionless J/κ and U/κ in two-site KH system with single-photon exchange. ζ and C_I are multiplied by 10^3 in the case of $F/\kappa = 0.1$ for visibility.

and the correlation time of the reservoir photons is negligibly short. Under these so called Born and Markov conditions, the dynamics of the open systems can be determined by solving the master equations

$$\dot{\hat{\rho}}^{(j)} = -i[\hat{H}^{(j)}, \hat{\rho}^{(j)}] + \sum_{i=1,2} \kappa_i \mathcal{D}[x]\hat{\rho}^{(j)}, \tag{3.6}$$

for both single ($j = 1$) and two photon ($j = 2$) exchange cases. Here, $\hat{\rho}^{(j)}$ is the density operator for the corresponding case; κ_i are the photon loss rates out of the cavities. $\mathcal{D}[x]\hat{\rho}^{(j)} = [2\hat{x}\hat{\rho}^{(j)}\hat{x}' - \hat{x}'\hat{x}\hat{\rho}^{(j)} - \hat{\rho}^{(j)}\hat{x}'\hat{x}]/2$ are the Liouvillian superoperators in the Lindblad form. We assume $\kappa_i \equiv \kappa$ and coherent pump amplitude F is taken to be real. Nonlinearity in our model Hamiltonians is assumed due to a Kerr type nonlinear material in the cavities and thus we can use the bare dissipation rates of the cavities in our treatment. Our generic models could effectively describe other systems

such as those of circuit QED in dispersive regime [103] or exciton-polariton systems of coupled cavity QED [69]. In such cases, canonical transformations used to obtain the effective models apply to the Lindblad noise terms and dressed dissipation rates must be used [69, 103].

We solve the master equation for the steady state density operator using the QuTiP: Quantum Toolbox in Python software [104]. The master equation is solved by taking $N_1 = N_2 = 4$ for the Fock space dimensions of each cavity field. When we increase the Fock space dimension up to 8 and remake our calculations, we find that the results remain unchanged. We consider two cases distinguished by the action of weak $F/\kappa = 0.1$ and strong pump $F/\kappa = 1$. We take $\kappa/2\pi = 0.4$ MHz. The parameters we use in the simulations are within the ranges accessible in present circuit QED systems [105, 106].

Numerically computed steady state density operator is used for calculation of second order coherence, spin squeezing, concurrence and mode entanglement parameters. Zero-time delay second order quantum coherence function is defined by [4]

$$g^{(2)}(0) = \frac{\mathrm{tr}(\hat{b}^\dagger \hat{b}^\dagger \hat{b}\hat{b}\hat{\rho})}{[\mathrm{tr}(\hat{b}^\dagger \hat{b}\hat{\rho})]^2}, \tag{3.7}$$

$$= 1 + \frac{\langle (\Delta\hat{n})^2\rangle - \langle \hat{n}\rangle}{\langle \hat{n}\rangle^2}, \tag{3.8}$$

Here $\hat{n} = \hat{b}^\dagger\hat{b}$, $\Delta\hat{n} = \hat{n} - \langle\hat{n}\rangle$; and we use ρ instead of $\rho^{(j)}$ for notational simplicity. We evaluate $g^{(2)}(0)$ for $\hat{b} = \hat{b}_i$. Both cavity photons have identical coherence functions due to exchange symmetry of our models under $b_1 \leftrightarrow b_2$. $g^{(2)}(0) < 1$ implies sub-Poissonian statistics of photons, while $g^{(2)}(0) > 1$ implies super-Poissonian statistics. Coherent photons are recognized by $g^{(2)}(0) = 1$. Sub-Poissonian statistics is a violation of the Cauchy-Schwartz inequality obeyed by classical light; and hence it is a profound manifestation of quantum light.

Spin squeezing is witnessed by the inequality [25]

$$\langle \hat{J}_k^2\rangle + \langle \hat{J}_l^2\rangle - \frac{N}{2} \leq (N-1)(\Delta\hat{J}_m)^2, \tag{3.9}$$

where k, l, m take all the possible permutations of x, y, z. Inequality given in Eq. (3.9) is one of the four optimal spin squeezing inequalities introduced in Ref. [25] with N being the total number of particles in the system. Violation of it implies spin squeezing and particle entanglement and its relation to the positivity of the concurrence can be found in Ref. [107]. We rewrite the optimal spin squeezing inequality given in Eq. (3.9) with $k = x, l = z$ and $m = y$ as

$$\zeta \equiv \langle \hat{J}_x^2 \rangle + \langle \hat{J}_z^2 \rangle - \frac{N}{2} - (N-1)(\Delta \hat{J}_y)^2 \leq 0. \tag{3.10}$$

The positive values of ζ indicate spin squeezing and multi-particle entanglement in the first quantization description. As we have an open system, $N = \langle \hat{N} \rangle = \langle \hat{n}_1 \rangle + \langle \hat{n}_2 \rangle$, with $\hat{N} = \hat{n}_1 + \hat{n}_2$ and $\hat{n}_i = \hat{b}_i^\dagger \hat{b}_i$, is not conserved and varies in time.

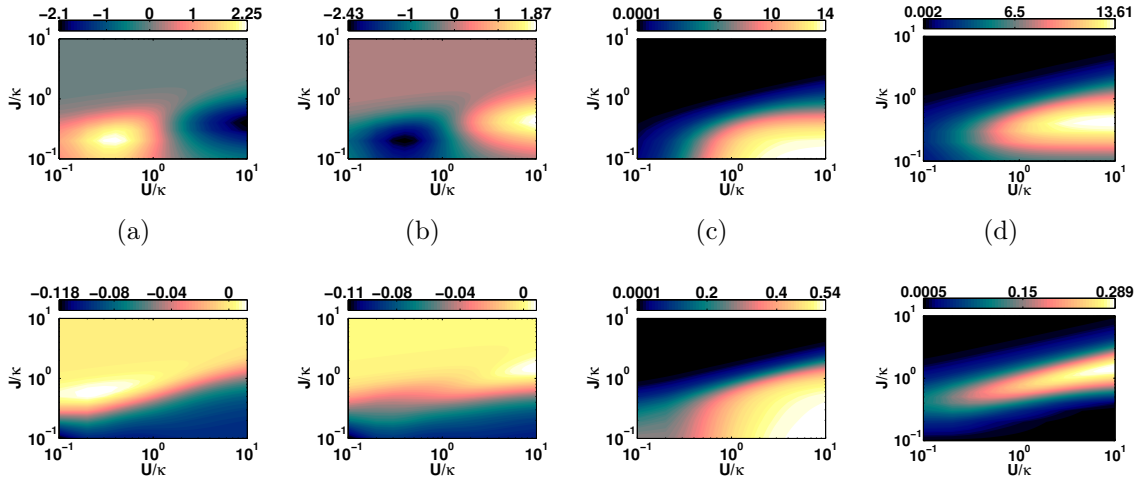

Figure 3-2: Dependence of (a) λ_1, (b) λ_2 (c) $S(\rho_1)$ for $F/\kappa = 0.1$ (d) $E_N(\rho)$ and (e) λ_1, (f) λ_2 (g) $S(\rho_1)$ (h) $E_N(\rho)$ for $F/\kappa = 1$ with respect to dimensionless J/κ and U/κ in two-site KH system with single-photon exchange. λ_1 and λ_2 are multiplied by 10^5, $S(\rho_1)$ is multiplied by 10^4, and $E_N(\rho)$ is multiplied by 10^3 in the case of $F/\kappa = 0.1$ for visibility.

In addition, we analyze pairwise particle entanglement through so called I-concurrence [87] given as

$$C_I = \sqrt{2(1 - \mathrm{tr}\rho_i^2)}, \tag{3.11}$$

where ρ_i with $i = 1, 2$ is the reduced density operator of the subsystem under consideration. $C_I = 0$ for product states and nonzero for entangled states. The maximum value of C_I cannot exceed $C_I^{max} = \sqrt{2(1 - 1/N)}$ where $N = 4$ is the Hilbert space dimension of the subsystem. For our case it is found to be $C_I^{max} \cong 1.225$.

We investigate the entanglement in the second quantized description in terms of the genuine two-mode entanglement parameters λ_1 and λ_2 given by [88, 89]

$$\lambda_1 = |\langle \hat{b}_1^\dagger \hat{b}_2 \rangle|^2 - \langle \hat{n}_1 \hat{n}_2 \rangle, \tag{3.12}$$

$$\lambda_2 = |\langle \hat{b}_1 \hat{b}_2 \rangle|^2 - \langle \hat{n}_1 \rangle \langle \hat{n}_2 \rangle, \tag{3.13}$$

where $\hat{n}_i = \hat{b}_i^\dagger \hat{b}_i$ with $i = 1, 2$. Positivity of the parameters λ_1 and λ_2 indicates mode entanglement. Positivity of the λ_1 and λ_2 is an only sufficient condition. On the other hand, their usability for the investigation of modal entanglement has recently been established [108].

The von Neumann entropy for the reduced density operator ρ_i with $i = 1, 2$ is given by [53]

$$S(\rho_i) = -\mathrm{tr} \rho_i \ln \rho_i. \tag{3.14}$$

The maximum value of the entropy is given by $S(\rho_i)^{max} = \ln N = \ln 4 \cong 1.386$. Its nonzero values detect the entanglement and is a measure for bipartite entanglement.

I-Concurrence and von Neumann entropy are reliable to characterize pairwise and bipartite entanglement in pure states. Steady states of our models may not be pure under strongly nonlinearity and strong drive. We calculate the impurity parameter $I = 1 - Tr(\rho^2)$ and report the plots of logarithmic negativity $E_N(\rho)$, which is applicable to mixed state bipartite entanglement. It is defined as [109]

$$E_N(\rho) = \log_2 ||\rho^{T_1}||_1, \tag{3.15}$$

where ρ^{T_1} is the partial transpose with respect to the first subsystem $i = 1$ and $||\rho^{T_1}||_1$ is the trace norm of ρ^{T_1}. Nonlinearity in our system and large Hilbert space dimensions make the calculation of other mixed state entanglement measures, which

are convenient for Gaussian states or states of finite dimensions, too difficult while $E_N(\rho)$ is a computable and non-convex entanglement monotone [110].

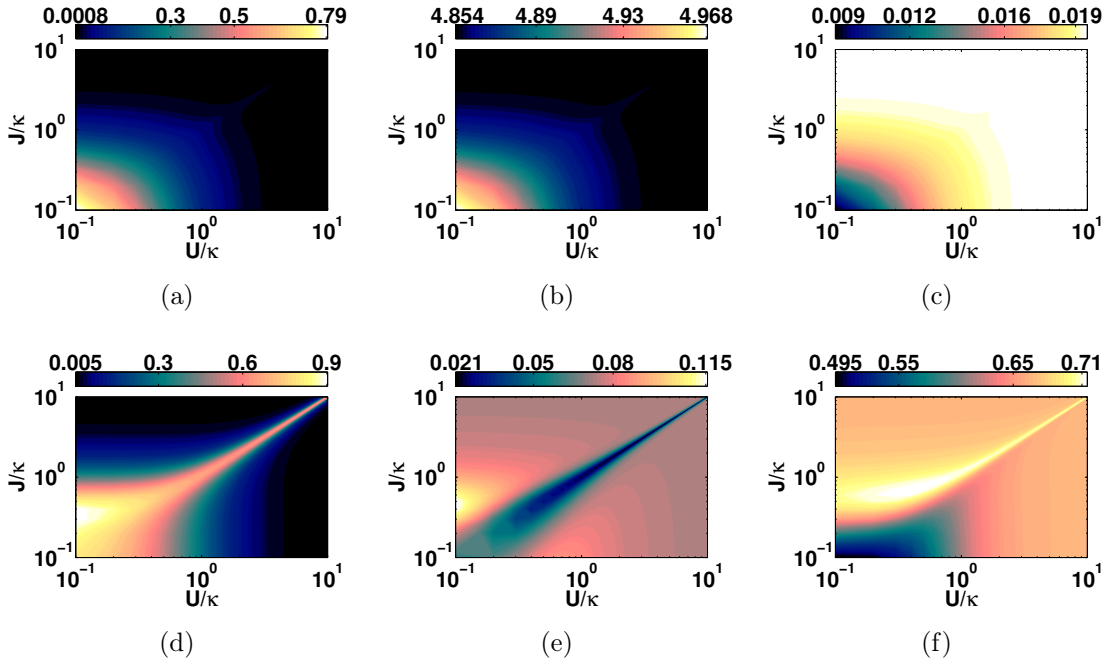

Figure 3-3: Dependence of (a) $g^{(2)}(0)$, (b) ζ (c) C_I for $F/\kappa = 0.1$ and (d) $g^{(2)}(0)$, (e) ζ (f) C_I for $F/\kappa = 1$ with respect to dimensionless J/κ and U/κ in two-site KH system with two-photon exchange. ζ is multiplied by 10^3 in the case of $F/\kappa = 0.1$ for visibility.

An intuitive link between coherence, particle and mode entanglements can be formed by considering that coherence function is a relative measure of number fluctuations which carries information on deviation from Poisson statistics. One can establish an analogy between the number operator $\hat{n}$ and the z-component of the angular momentum operator $\hat{J}_z$ using $\hat{n}_1 = \hat{N}/2 + \hat{J}_z$. The coherence function is influenced by squeezing the spin noise around the z axis. Under stringent conditions spin squeezing implies particle entanglement. Particle like behavior, enforced by the sub-Poissonian statistics can be associated with spin squeezing type pairwise nonlinear interactions. In that case coherence and spin squeezing interplay can be further extended to multiparticle entanglement. Similarly λ_1 and λ_2 can be expressed in terms of spin fluctuations and thus would be influenced by the coherence and spin

squeezing in the system.

Above heuristic arguments motivates the existence of an interplay between coherence, particle and mode entanglement. Let us now analyze specific cases numerically. We will first consider the single photon exchange case, then proceed to two photon exchange case in the following subsections.

3.2.1 Single-Photon Exchange

In Fig. 3-1(a), Fig. 3-1(b) and Fig. 3-1(c) we plot second order coherence, spin squeezing and concurrence parameters as functions of nonlinearity and photon exchange coefficients in the case of weak drive with $F/2\pi = 0.04$ MHz, respectively. Fig. 3-1(a) reproduces the result in Ref. [69]. Second order coherence varies over the range of $0.00183 \leq g^{(2)}(0) \leq 1.011$. Coherent delocalization of cavity photons happens for $J/\kappa > 1$ and $J > U$, which corresponds to the Poissonian statistics indicated by $g^{(2)}(0) \sim 1$. Strong sub-Poissonian localization regime with $g^{(2)}(0) \sim 0$ lies in the region of $U/\kappa > 1$ and $J/\kappa < 1$.

Fig. 3-1(b) shows that spin squeezing always present in the system for the ranges of $0.1 < U/\kappa, J/\kappa < 10$. Pairwise nonlinearity measured by U in the driven system is strong enough for the survival of multiparticle entanglement in the steady state. It is easier to violate spin squeezing inequality in the region of $J/\kappa < 1$, where sub-Poissonian and hence particle like behavior is more significant. This is intuitively expected as the delocalizing photon hopping makes particle entanglement more difficult, while nonlinear interaction favors particle correlations.

Fig. 3-1(c) shows that the pairwise entanglement characterized with concurrence is in agreement with the spin squeezing. It reaches its maximal value in the strong Sub-Poissonian regimes, where particle entanglement is maximal.

Fig. 3-1(d), Fig. 3-1(e) and Fig. 3-1(f) depict quantum coherence, spin squeezing and concurrence for the case of strong drive of $F/2\pi = 0.4$ MHz, respectively. Coherent effects of the drive is harmful for the particle like character and the range of $g^{(2)}(0)$ is shifted away from 0 and becomes $0.00486 \leq g^{(2)}(0) \leq 1.0321$. Stronger nonlinearity is needed for sub-Poissonian statistics and thus the region is narrowed in

the U/κ axis relative to that in Fig. 3-1(a). Multiparticle and pairwise entanglement becomes harder to establish relative to weak drive case. The maximum values of ζ and C_I reduce about an order of magnitude when the coherent drive is increased an order of magnitude. Spin squeezing and concurrence are almost absent in the super-Poissonian region. Mode entanglement parameter λ_1 behavior with J and U, shown

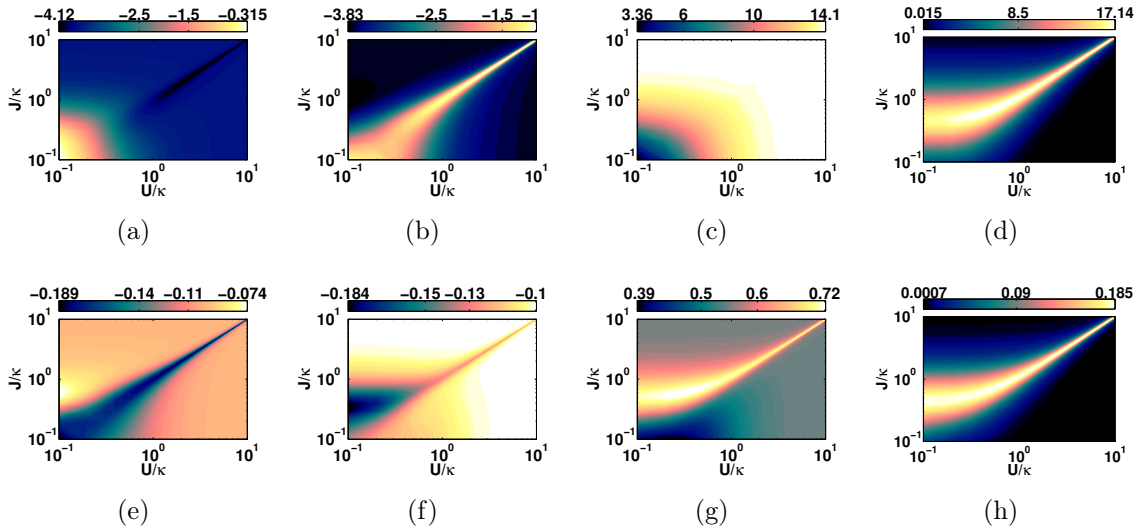

Figure 3-4: Dependence of (a) λ_1, (b) λ_2 (c) $S(\rho_1)$ for $F/\kappa = 0.1$ and (d) λ_1, (e) λ_2 (f) $S(\rho_1)$ for $F/\kappa = 1$ with respect to dimensionless J/κ and U/κ in two-site KH system with two-photon exchange. λ_1 and λ_2 are multiplied by 10^5, $S(\rho_1)$ is multiplied by 10^4, and $E_N(\rho)$ is multiplied by 10^3 in the case of $F/\kappa = 0.1$ for visibility.

in Fig. 3-2(a), is opposite to that of spin squeezing and concurrence. Localization of photons in the cavities favor pairwise particle entanglement; while wave like behavior associated with coherent delocalization by the photon exchange favors mode correlations. The behavior of the parameter λ_2, shown in the Fig. 3-2(b), indicates that the mode entanglement occurs in the nonlocal regimes with strong nonlinearity. Fig. 3-2(e) and Fig. 3-2(f) show the mode entanglement parameters for the case of strong drive of $F/2\pi = 0.4$ MHz. Here, mode correlations become harder to establish and regions where the modes are entangled are shifted towards higher J/κ values.

Fig. 3-2(c) and Fig. 3-2(g) show the dependence of the von Neumann entropy for weak $F/2\pi = 0.04$ MHz and strong $F/2\pi = 0.4$ MHz drive conditions, respectively. Bipartite entanglement almost absent in the hopping dominant regimes, whereas the

entropy reaches its maximal value in nonlinearity dominant regimes.

Fig. 3-2(d) and Fig. 3-2(h) show the behavior of logarithmic negativity $E_N(\rho)$. The impurity parameter for the weak drive case is calculated to be in the range $I \sim 0 - 10^{-4}$ while it becomes $I \sim 0 - 0.36$ for the strong drive case. We do not plot I as it behaves as $g^{(2)}$. In the single photon exchange model, steady state is more pure in regions with greater Poissonian character. Only under strong drive and strong nonlinearity, where $I \sim 0.2 - 0.36$, characterization of the entanglement with C_I and $S(\rho_1)$ can be ambiguous. In this case existence of entanglement is confirmed by E_N.

Behaviors of the genuine mode entanglement parameters λ_1 and λ_2 along with the von Neumann entropy give a complete description of mode correlations. First, occurrence of two-mode correlations in the sub-Poissonian regions is typical for two-squeezed light beams mixed with a beam splitter. Here, this happens simultaneously, not sequentially. Second, the von Neumann entropy covers the whole region which covered separately by the mode-entanglement parameters. Bipartite entanglement is distributed over sub-Poissonian regimes.

We stressed out that the single photon exchange model gives clearly distinct roles to the interactions. Nonlinearity is localizing and a single-axis twisting spin squeezing type of interaction. Photon hopping is delocalizing and a mode correlating interaction. Two photon hopping however has particle and delocalizing character. It is delocalizing due to photon exchange effect, but also establishes pairwise correlations by a two axis twisting interaction. We will point out emergence of distinct relation between second order coherence and entanglement in the following subsection.

3.2.2 Two-Photon Exchange

In Fig. 3-3 and Fig. 3-4, we show our results for two-photon exchange interaction. Fig. 3-3(a), Fig. 3-3(b) and Fig. 3-3(c) depict quantum coherence, spin squeezing and concurrence for $F/2\pi = 0.04$ MHz, respectively. In contrast to single photon exchange, there is no Poissonian or super-Poissonian region in Fig. 3-3(a) and $g^{(2)}(0)$ varies in the range of $0.00723 \leq g^{(2)}(0) \leq 0.7944$. The sub-Poissonian statistics is

strong in both delocalizing photon hopping and local cavity nonlinearity dominated regimes. Relatively weak one occurs in $J/\kappa, U/\kappa < 1$ region where coherent drive is comparable to these local and nonlocal pairwise interactions.

In the two photon exchange case, analogous to LMG model, there are both single axis and two axis twisting routes to spin squeezing. When $J/\kappa > 1$ the former becomes the major route leading to spin squeezing; while when $U/\kappa > 1$ the latter becomes the main interaction causing spin squeezing. Accordingly strong violation of spin squeezing occurs over the entire domain of $J/\kappa, U/\kappa$. Similar level of violation can only be found in the narrow strip of weak J/κ in Fig. 3-1(b). The uniformity of the pairwise entanglement witness parameter with U which is present in Fig. 3-1(b) is no longer present in Fig. 3-3(b). Variation of spin squeezing and sub-Poissonian statistics strength with hopping and nonlinearity becomes identical for the case of two photon exchange. As in the single-photon interaction case, concurrence is in complete agreement with spin squeezing. In both nonlinearity and hopping dominated regimes pairwise particle correlations show identical statistical character. Particle entanglement is maximized for $J/\kappa \gtrsim 1$ and $U/\kappa \gtrsim 1$.

Fig. 3-3(d), Fig. 3-3(e) and Fig. 3-3(f) show quantum coherence, spin squeezing and concurrence for $F/2\pi = 0.4$ MHz, respectively. Strong drive helps to bring coherence into the system and now the maximum $g^{(2)}(0) \sim 1$. The separation of two strong sub-Poissonian regions by a weak one around the line $J = U$ becomes more visible. Strong drive works against spin squeezing that reaches its maximum value around $J/\kappa \sim 0.5 > U/\kappa$. Concurrence is maximized around similar J/κ values as spin squeezing with relatively strong nonlinearity.

In Fig. 3-4, we plot the mode entanglement and entropy parameters for the two-photon exchange interaction. Being only sufficient, values of the parameters λ_1 and λ_2 within our parameter regimes make the discussions on mode entanglement inconclusive [108].

Fig. 3-4(c) shows the von Neumann entropy for the case of $F/2\pi = 0.04$ MHz. Bipartite entanglement is strong in both local and nonlocal interaction regimes. In the case of strong pump, shown in Fig. 3-4(f), it is maximized in the diagonal which

separates two weaker regimes. This diagonal corresponds to the weaker multiparticle but stronger pairwise entanglement situations depicted in Fig. 3-3(e) and Fig. 3-3(f), respectively.

Fig. 3-4(d) and Fig. 3-4(h) show the behavior of logarithmic negativity $E_N(\rho)$. The impurity parameter for the weak drive case is calculated to be in the range $I \sim 10^{-5} - 10^{-4}$ while it becomes $I \sim 0.22 - 0.39$ for the strong drive case. We do not plot I as it behaves as $g^{(2)}$. In the two-photon exchange model, similar to the single photon exchange case, steady state is more pure in regions with greater Poissonian character. In contrast to single photon exchange case however, mixed state region with $I \sim 0.2 - 0.36$ is not limited to strong nonlinearity but extends over the entire region under strong drive and hence characterization of the entanglement with C_I and $S(\rho_1)$ can be ambiguous. In this case existence of entanglement is confirmed by E_N.

Two-photon exchange between weakly driven identical nonlinear cavities make the photons strongly antibunched for any J and U, except for weak J and U quadrant where photons have weaker sub-Poissonian character. Single photon exchange can only generate antibunched photons for $J < U$ and coherent photons for $J > U$ [69]. A strong drive is most influential to enhance the coherence regime for two photon hopping case when $J \sim U$.

Our analysis reveals viable routes to entanglement realization in our models. Coherence serves as a map to search for most advantageous J and U domains for practical establishment of entanglement. Under weak drive, antibunched photons in single photon exchange violate the product state conditions $3 - 5$ orders of magnitude more strongly than the super-Poisson ones. Two-photon exchange yields almost uniform violation with similar but maximum quantum noise levels. This points out one crucial advantage of two photon exchange over the single photon exchange for practical realization of entanglement. There are both single and two-axis twisting spin squeezing routes to entanglement in two-photon exchange which leads to almost uniform and strong satisfaction of particle, pairwise and mode entanglement conditions over the entire J, U domain. There is another surprising and appealing advantage in the

two-photon exchange under strong drive. Entanglement emerges most easily in weak nonlinearity and weak hopping region and with photons of relatively weak sub-Poisson character.

For both single and two-photon exchange, multi-particle entanglement is harder to establish relative to pairwise and mode entanglements, which are at similar levels of quantum noise. Quantum fluctuations could be too low to detect in experiments for all types of entanglements under weak drive. Strong drive remedy this situation and increases quantum fluctuations $1-2$ orders of magnitude more in steady state. Strong drive also leads to mixed state entanglement, albeit with weak mixedness, in the sub-Poisson regime of single photon exchange or everywhere in two-photon exchange.

THIS PAGE INTENTIONALLY LEFT BLANK

Chapter 4

Discrete time quantum walk with nitrogen-vacancy centers in diamond coupled to a superconducting flux qubit

Spin ensembles that are coupled to quantum electrodynamics (QED) systems and solid-state qubits are promising hybrid architectures [111] for quantum memories [112] and for distributed quantum networking [113]. Nitrogen-vacancy (NV) centers in diamond are outstanding among the solid-state spin ensembles [114] due to their long spin relaxation and dephasing times, scalability [115] and existence of well-established techniques for their manipulation [116, 117, 118]. NV center quantum memory has recently been demonstrated [119].

Quantum memories require fast and reliable quantum state transfer, which is closely related to the quantum walk (QW) problem [120, 121, 122]. In particular, the discrete time QW (DTQW) [123, 124, 121, 125] has been highlighted for universal quantum computation [126] and for quantum state transfer [127]. NV centers that are coupled to superconducting transmission line resonators are considered before for continuous-time QW [128]. Here we propose a scheme for implementing DTQW with

NV centers.

Our scheme is based upon the proposals for DTQW in phase space introduced for cavity QED (CQED) [129, 130, 11] and circuit QED (cirQED) [131]. Like some other intriguing proposals [132, 133, 134], QWs in CQED and cirQED schemes have not been demonstrated yet; despite some successful realizations in different systems [135, 136, 137, 138, 139, 140]. Our procedure could lead to the first solid-state realization of the proposed DTQW in phase space.

We consider an NV center ensemble coupled to a superconducting flux qubit [141], which plays the role of the coin in DTQW. Weak excitations of NV centers can be described in terms of bosonic quasiparticles. We take into account all the crystallographic classes of the NV centers so that the single mode coupled to the qubit becomes an effective privileged mode, which is a particular superposition of all the modes corresponding to the quasiparticle excitations in four different NV center crystallographic classes. We derive an exact bilinear spin-boson model that reduces to Jaynes-Cummings model (JCM), same with that in CQED or cirQED settings, under parametric approximation.

We employ the similar but improved DTQW scheme proposed for JCM to our case, by removing the cumbersome requirement of varying drive-pulse durations. This allows for the direct realization of DTQW with regular time steps and simplifies the implementation in all indirect-coin-flip cavity QED realizations of QW including our full solid-state proposal.

4.1 Model System

4.1.1 NV center ensemble Hamiltonian

A theoretical model of NV centers in diamond can be developed based on the six-electron description of the ^3A electron spin triplet ground state of NV^- [142, 143]. The hyperfine (~ 2 MHz for ^{14}N), quadrupole (~ 5 MHz for ^{14}N), and strain (< 10 MHz) interactions are negligible [144] relative to zero-field splitting ~ 2.88 GHz. Similar

conclusion is applicable to ^{13}C as well [145]. The Hamiltonian of a single NV center in the absence of external electric and magnetic fields can be written as [146, 147]

$$H = \tilde{S}^T \tilde{D} \tilde{S}, \tag{4.1}$$

where $\tilde{S}$ is the spin-1 matrix and $\tilde{D}$ is the zero-field splitting matrix. The NV center Hamiltonian in the principal axes of the molecular body frame becomes diagonal so that

$$H = D\left[S_z^2 - \frac{1}{3}S(S+1)\right], \tag{4.2}$$

where $S = 1$ and $D/2\pi \approx 2.88$ GHz [148]. By taking the quantization axis z as the alignment of the NV center, the Hamiltonian can be expressed in the spin basis $|S, m\rangle \equiv |m\rangle$ as

$$H = D\sum_{m=\pm 1,0} m^2 |m\rangle\langle m|, \tag{4.3}$$

where we dropped the constant term.

There are four possible quantization axes in the NV center, which are all equivalent. We need to take them into account when we consider an ensemble of NV centers. Let us denote these axes by $f = 1, \ldots, 4$ and introduce collective operators, which are analogs of Hubbard operators for strongly correlated electron systems [149], such that

$$X_f^{mn} = \sum_{j=1}^{N_f} |m\rangle_j^{(f)} \langle n|_j^{(f)}. \tag{4.4}$$

Here, $|\, m\rangle_j^f$ is the spin state of the j-th NV center aligned along the crystallographic (molecular) axis-f which is taken as the quantization axis. N_f denote the number of NV centers aligned along the quantization axis f. The Hamiltonian for the NV

center ensemble becomes

$$H_{\mathrm{NV}} = D \sum_{mf} m^2 X_f^{mm}. \tag{4.5}$$

4.1.2 Flux qubit Hamiltonian

A flux qubit consists of three or more superconducting Josephson junctions, one of which is smaller than the others [150, 151]. The phase quantization condition for the superconducting wave functions around the qubit loop reduces the system to a two-dimensional phase space, where the qubit can be effectively considered as a two-particle system subject to a double-well potential [152]. A two-level approximation can be made to the band structure of the potential by assuming that the external flux is in the vicinity of half of the flux quantum, where the two lowest bands are closest to each other. A small overlap of the wave functions of the two levels opens the qubit gap Δ_q, which can be tuned [153, 154, 155] by replacing the smallest Josephson junction with two parallel junctions, a DC-SQUID. On the basis of the two counter-rotating persistent currents in the qubit loop, the qubit Hamiltonian can be written as

$$H_q = \frac{1}{2} \left(\Delta_q \sigma_x + \epsilon_q \sigma_z \right), \tag{4.6}$$

where ϵ_q is the magnetic energy bias of the qubit that contributes away from the symmetry point, when there is a net persistent current in the qubit loop.

Pauli spin operators $\sigma_{x,y,z}$ can be conveniently transformed from the bare current basis to the dressed current basis by $U = \exp\left(-i\theta\sigma_y\right)$ with $\theta = \arctan\left(\Delta_q/\epsilon_q\right)$. The Hamiltonian becomes

$$H_q = \frac{\omega_q}{2} \sigma_z, \tag{4.7}$$

with the qubit frequency $\omega_q = \sqrt{(\Delta_q^2 + \epsilon_q^2)}/2$.

4.1.3 Flux qubit-NV ensemble coupling

We assume the same conditions as in a recent experiment [156], wherein the flux qubit was coupled to the NV center ensemble located at the top of the central region of the flux qubit loop. The dimensions of the ensemble are sufficiently small for the spatial variations in the magnetic field over the ensemble to be ignored. In such a case, the magnetic fields generated by the supercurrents are expected to interact with the ensemble homogeneously. In the persistent current basis the electronic Zeeman interaction is given by

$$H_{\text{int}} = \sum_{\alpha=x,y,z} g_{\alpha}^{f} S_{f}^{\alpha} \sigma_{z}, \tag{4.8}$$

where S_f^α are the total spin-1 operators for the NV ensemble that are related to the generators of the SU(3). Nuclear Zeeman interaction is three orders of magnitude smaller and neglected. Here, α denotes the coordinate in the molecular body frame; and σ_z is associated with the magnetic field in the persistent current basis.

The electronic Zeeman interaction is diagonal in the molecular body frame. The symmetry axes $\langle 111 \rangle = [11\bar{1}], [111], [1\bar{1}1], [\bar{1}11]$, shown in Fig. 4-1, which correspond to four crystalographic classes $f = 1, 2, 3, 4$, respectively, are taken to be the z axes of the molecular body frames. The coupling strengths $g_\alpha^f = 2g_e\mu_B B_{f\alpha}$, where g_e is the electronic Landé g factor, μ_B is the Bohr magneton and $B_{f\alpha}$ is the α-component of the magnetic field acting in the molecular frame of the crystallographic class f, can be adjusted by the orientation of the diamond sample. In a typical experimental setting [156], the crystal axis [001] is parallel to the magnetic field. The crystal surface (001) is perpendicular to the magnetic field and placed on top of the flux qubit.

If we take the [001] direction as the crystal lab frame z axis, then the Zeeman interaction coefficients become proportional to the direction cosines of the lab and body frame z axes. The angle between the $f = 1$ and $f = 2$ axes and the angle between the $f = 3$ and $f = 4$ axes are the same in the diamond unit cell. The magnetic field axis bisects them and thus the magnetic field makes the same angle of 54.7° with the every body frame z axes. The molecular body frames are chosen such

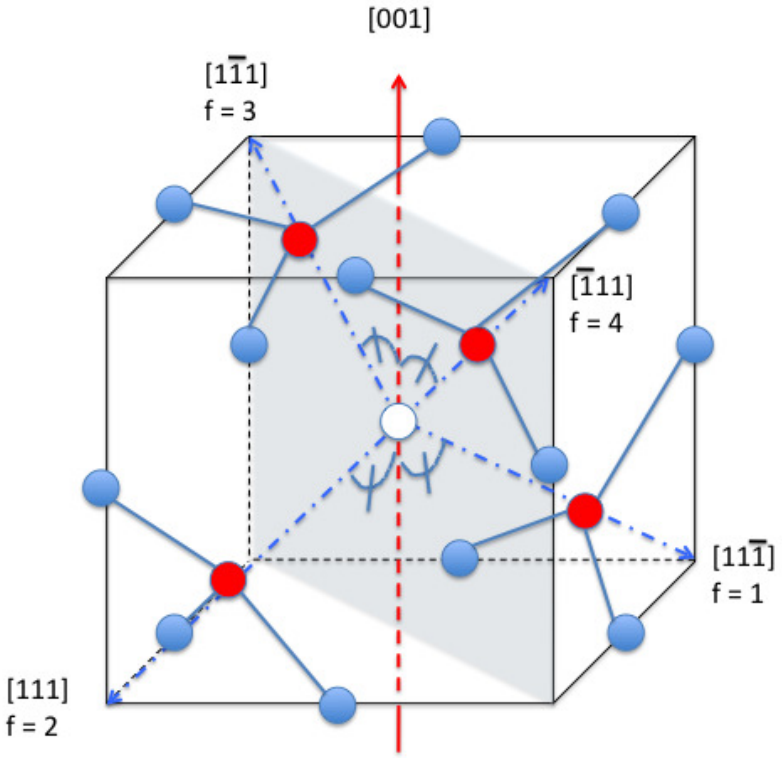

Figure 4-1: Four equivalent crystallographic groups of the NV centers. Symmetry axes $\langle 111 \rangle$ make the same angle with the magnetic field parallel to the axis directed along [001]. The blue spheres along the sides of the cube represent the C atoms; the white sphere at the center represents the vacancy; the red spheres along the $\langle 111 \rangle$ axes represent the N atoms. We use the short hand notation $f = 1, 2, 3, 4$ for the axes $[11\bar{1}], [111], [1\bar{1}1], [\bar{1}11]$, respectively.

that the y axes are perpendicular to the magnetic field and the x axes make an angle of 35.3° with the magnetic field. This makes $g_\alpha^f = g_\alpha$ the same for all crystallographic classes f and g_z, associated with the smaller direction cosine, becomes smaller relative to g_x while $g_y = 0$ [141, 156]. These lead to the reduced interaction of the form

$$\begin{aligned} H_{\text{int}} = \; & \textstyle\sum_f \sigma_z [g_x (X_f^{-0} + X_f^{+0} + \text{H.c.}) \\ & + g_z (X_f^{++} - X_f^{--})], \end{aligned} \tag{4.9}$$

where H.c. stands for Hermitian conjugate. Here we replaced the collective spin operator by the analogs of the Hubbard operators introduced in Eq. (4.4) such that $S_x^f = X_f^{-0} + X_f^{+0} + X_f^{0-} + X_f^{0+}$ and $S_z^f = X_f^{++} - X_f^{--}$.

We shall proceed under the assumptions of weak excitations and a large number of spins in the ensemble. Experiments can achieve coupling of $N \sim 3.1 \times 10^7$ NV centers directly above the flux qubit [156]. This number is sufficiently large for our weak-excitation conditions. We consider about $5-10$ excitations in our simulations. Under these conditions, operators X_f^{mn} can be conveniently related to bosonic operators x_{fm} such that

$$X_f^{mn} = x_{fm}^\dagger x_{fn}, \tag{4.10}$$

in terms of which the corresponding terms in the Hamiltonian $H = H_{\rm NV} + H_q + H_{\rm int}$ becomes

$$H_{\rm NV} = D \sum_{mf} m^2 x_{fm}^\dagger x_{fm}, \tag{4.11}$$

$$H_{\rm int} = \sum_f g\sigma_z (x_{f-}^\dagger x_{f0} + x_{f+}^\dagger x_{f0} + \text{H.c.}), \tag{4.12}$$

where we neglected $g_z(x_{f+}^\dagger x_{f+} - x_{f-}^\dagger x_{f-})$ and redefined $g_x := g$ in Eq. (4.12). The operators x_{fm} play the role of Schwinger bosons of $SU(N_f)$ subject to the constaint $\sum_m \langle x_{fm}^\dagger x_{fm}\rangle = N_f$ [157, 158, 159]. Schwinger bilinear boson representation of the Hubbard operators preserve their algebra. The algebraic relations are summarized in Appendix 4.3.1.

The quasiparticles of NV center excitations are analogous to quantum particles associated with the spin waves, and hence, we call them quasimagnons. We introduce quasimagnon operators as follows: $x_{f+} \equiv a_f, \quad x_{f-} \equiv b_f$, and proceed by replacing $x_{f0} \to \sqrt{N_f}$ which is analogous to the parametric pump approximation in quantum optics [160]. Parametric approximation has quite a wide range of validity, which is especially enhanced for initially coherent states [161]. To the first order the error is as large as the of the square root of the mean quasimagnon number. Fractional error,

relative to the mean number of quasimagnons, is about the size of relative fluctuation which is negligible in our case $\sqrt{N}/N \sim 0.01$. The change from the algebra preserving Schwinger bosons to quasimagnons by the parametric aproximation is equivalent to deforming the Holstein-Primakoff map under group contraction by large total spin approximation [162].

We consider initially coherent spin ensembles for our quantum walk procedure as well, which could make our procedure potentially applicable for higher number of excitations, or equivalently for smaller number of NV centers coupled to the flux qubit. A systematic study of how tolerant our procedure to smaller number of NV centers however needs further examinations without parametric approximation, which is beyond the scope of our present investigations.

The Hamiltonian of the NV centers then reduces to

$$H_{\mathrm{NV}} = \sum_f D(a_f^\dagger a_f + b_f^\dagger b_f). \tag{4.13}$$

We interpret the presence of two quasimagnon operators by associating them with quasispin waves with two possible polarizations. The final Hamiltonian is then an eight-mode model, in which there are four quasimagnon modes, each with two different polarization degrees of freedom.

By employing the rotating wave approximation for $g \ll D, \omega_q$, transforming to the dressed current basis at the qubit symmetry point, and using the quasimagnon picture, we can express the interaction as

$$H_{\mathrm{int}} = \sum_f [\eta_f(\sigma_+(a_f + b_f) + \sigma_-(a_f^\dagger + b_f^\dagger)], \tag{4.14}$$

with $\eta_f = g\sqrt{N_f}$ being the collective coupling strengths for the quasimagnons and flux qubit system. Here $\sigma_\pm = \sigma_x \pm \mathrm{i}\sigma_y$ are the Pauli spin ladder operators.

This Hamiltonian can be simplified by distinguishing sets of “coupled modes" and “uncoupled modes," analogous to Morris-Shore transformations [163], which are combinations of quasimagnon modes such that they are respectively interacting and

noninteracting with the flux qubit. We list these modes in Appendix 4.3.2. Eventually, only a single effective privileged mode becomes coupled to the qubit. The annihilation operator of that mode is given by

$$c = \frac{1}{\sqrt{2N}} \sum_f \sqrt{N_f}(a_f + b_f). \tag{4.15}$$

The interaction Hamiltonian is then simplified to the usual Jaynes-Cummings model, though the single privileged (bright) mode is actually a spesific superposition of all the quasimagnon modes,

$$H_{\text{int}} = \eta(\sigma_+ c + \sigma_- c^\dagger), \tag{4.16}$$

where the collective spin-qubit coupling strength is $\eta = \sqrt{2N}g$. We ignore the effects of inhomogenous broadening and spatial inhomogeneity here and provide a brief discussion in Appendix 4.3.3.

4.1.4 Quantum walk Hamiltonian

We introduce an additional term that represents the driving field on the diamond sample

$$H_d = \epsilon(t)(ce^{i\omega_d t} + c^\dagger e^{-i\omega_d t}), \tag{4.17}$$

where ω_d is the drive frequency and $\epsilon(t)$ is the time-dependent amplitude of the drive pulse. Consistent with our spatial homogenity of the interaction assumption, the drive field is coupled with the quasimagnon mode defined in Eq. (4.15). We assume that the drive is of square-wave form with pulse duration t_H and amplitude ϵ_0. The total Hamiltonian of the qubit ensemble becomes the Jaynes-Cummings model Hamiltonian such that

$$H = \frac{\omega_q}{2}\sigma_z + Dc^\dagger c + \eta(\sigma_+ c + \sigma_- c^\dagger) + H_d(t). \tag{4.18}$$

This Hamiltonian is the same as that proposed for a QW in cirQED, although in our case, the role played by the microwave photons is assumed by the quasimagnons. Here, the qubit-NV center ensemble coupling η is about $\eta/2\pi \sim 70$ MHz [156]. In contrast to spontaneous decay and the dephasing of the qubit, the qubit-NV center ensemble interaction is in the strong-coupling regime. By employing a rotating frame transformation $H_R = U^\dagger H' U - \Lambda$ with $U = \exp(-i\Lambda t)$, where we take $\Lambda = \omega_d(c^\dagger c + \sigma_z/2)$, the Hamiltonian can be written in the form

$$H = -\delta_c c^\dagger c - \delta_d \frac{\sigma_z}{2} + \eta(c^\dagger \sigma_- + c\sigma_+) + \epsilon(c + c^\dagger). \tag{4.19}$$

Here, $\delta_d = \omega_d - \omega_q$ and $\delta_c = \omega_d - D$ are introduced.

The detuning between the qubit and the NV center ensemble is $\Delta = \delta_d - \delta_c = D - \omega_q$, which can be adjusted by ω_q to satisfy $\Delta \gg \eta$ so that the Fröchlich canonical transformation [164, 165, 166] $H' = \exp(-S) H \exp(S)$, with the transformation operator

$$S = \frac{\eta}{\Delta}(\sigma_- c^\dagger - \sigma_+ c), \tag{4.20}$$

can be applied to obtain an effective Hamiltonian

$$\begin{aligned} H_{\text{eff}} &= \chi c^\dagger c \sigma_z + \frac{\Omega_R}{2}\sigma_x + \epsilon(c + c^\dagger) - \delta_c c^\dagger c - \frac{\delta_d}{2}\sigma_z \\ &+ \frac{\chi}{2}(1_2 + \sigma_z), \end{aligned} \tag{4.21}$$

where 1_2 is the 2×2 unit matrix; and the parameters

$$\chi = \frac{\eta^2}{\Delta}, \quad \Omega_R = \frac{2\eta\epsilon(t)}{\Delta} \tag{4.22}$$

are associated with the conditional rotational shift and the Hadamard coin terms in the Hamiltonian. The Hadamard coin term only operates when the pulse is on, whereas the shift operation is constantly active. The conditional shift operator

$R(\chi) := \exp(\mathrm{i}\chi c^\dagger c\sigma_z)$ rotates the phase states

$$|\phi\rangle = \frac{1}{\sqrt{M}} \sum_{n=0}^{M-1} \mathrm{e}^{\mathrm{i}n\phi} |n\rangle , \tag{4.23}$$

on the phase space such that $R(\chi)|\phi\rangle|\sigma\rangle_z = |\phi + \sigma\chi\rangle|\sigma\rangle_z$. The rotation can be clockwise or counterclockwise depending on the state of the qubit $|\sigma = \pm 1\rangle_z$. Here $|n\rangle$ are the Fock states in an Hilbert space of dimension M. The conditional rotation is restricted to a cycle whose radius is determined by the mean quasimagnon number $\langle n_c\rangle = \langle c^\dagger c\rangle$ and the phase space coordinates correspond to the mean quadratures $\langle c + c^\dagger\rangle/2$ and $\langle (c - c^\dagger)\rangle/2\mathrm{i}$. The effect of the conditional rotation operator on a coherent state $|\alpha\rangle$ is similar; it translates the phase θ_α of the coherence parameter $\alpha = |\alpha| \exp(\mathrm{i}\theta_\alpha)$ to $\theta_\alpha \pm \chi$.

We note that in the QW proposal for cirQED, the parameter Ω_R is found to depend on ω_d by the relation $\Omega_R = 2\eta\epsilon(t)/\delta_c$. The dependence of Ω_R on the drive frequency results in a QW with varying step sizes in time, and complicated pre-adjustments in pulse duration are therefore required. Here, we do not have a drive-frequency-dependent coin operation and we have a fixed step size as well as fixed pulse duration. This makes the implementation of the QW more straightforward. In contrast to our approach described here, a displaced frame transformation relative to the resonator field was previously used in the cirQED model of a bit-flip gate [167], in addition to the Fröchlich transformation. This lead to vanishingly small cavity photon numbers and negligible ac Stark shifts. In our approach, we do not use a displaced frame, which allows for the presence of a larger number of quasimagnons.

4.2 Results and Discussion

The dynamics of the effective Hamiltonian is subject to decoherence processes. By denoting the qubit dephasing rate as γ_ϕ, the qubit relaxation rate as γ_1, and the decay of the NV center excitations as Γ, we can write the quantum master equation of the system, under the Markovian and Born-Markov approximations, which are suitable

for our weakly coupled system [168], as

$$\dot{\rho} = -i[H, \rho] + \Gamma\mathcal{D}[c]\rho + \gamma_1\mathcal{D}[\sigma_-]\rho + \frac{\gamma_\phi}{2}\mathcal{D}[\sigma_z]\rho. \tag{4.24}$$

Decoherence processes associated with an operator $x = c, \sigma_-, \sigma_z$ are described by the Liouvillian superoperators $\mathcal{D}[x]\rho = (2x\rho x^\dagger - x^\dagger x\rho - \rho x^\dagger x)/2$ in Lindblad form. We introduced the effective Hamiltonian to illustrate the underlying QW dynamics, but obtain quantitative results from the Hamiltonian of the system given in Eq. (4.19).

We do not simulate the effective Hamiltonian to avoid further approximations. The effective Hamiltonian only serves to interpret and design the dynamics of the system.

We solve the master equation using the QuTip package [169] in PYTHON software. The initial condition is considered to be

$$|\psi(0)\rangle = |\alpha\rangle(|g\rangle + i|e\rangle)/\sqrt{2}, \tag{4.25}$$

where the quasimagnons are in a coherent state with amplitude α and the qubit is in a superposition of its ground and excited states. It is assumed that excitations of the NV center ensemble is initially prepared in a coherent state. We consider a Fock space of quasimagnons with the dimension 17, which is sufficiently large to accommodate the selected $\alpha = 3$ in the numerical analysis. A classical magnetic field pulse can be used to prepare the quasimagnon coherent state analogous to the typical driven oscillator case [170], as for large number of NV centers the atomic coherent states converges to the bosonic coherent states [171]. The modes to be included in the initial coherent state could be selected by external bias magnetic fields. The initial coherent superposition of the flux qubit levels can be generated by a resonant magnetic pulse of area π.

Most of the parameters we use in our simulations can be taken as the same values with those used in the original circuit QED and cavity QED proposals [131, 11] except γ_1, Γ, D and ϵ_0. Flux qubit has a wide range of tunability and we set its gap frequency as $\omega_q/2\pi = 7$ GHz [151]. Recently developed flux qubits can have dephasing times in

the order of few microseconds [172] and we set $\gamma_\phi/2\pi = 0.31$ MHz. Recent experiments allow for direct coupling between the flux qubits and the NV centers with strengths of about ~ 70 MHz [156]. Number of NV centers and the flux qubit size can be used to control the strength of the coupling, which is taken here as $\eta/2\pi = 100$ MHz.

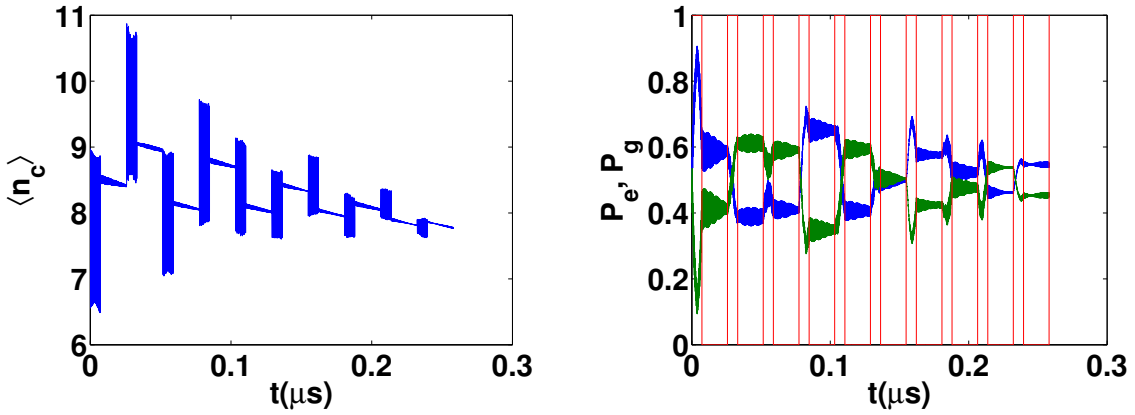

(a) (b)

Figure 4-2: (a) Time (t) dependence of the mean number of quasimagnons $\langle n_c \rangle$ and (b) of the qubit-level populations $P_{e,g}$ for the initial state $|\psi(0)\rangle = |\alpha = 3\rangle(|g\rangle + i|e\rangle)/\sqrt{2}$. $\langle n_c \rangle$ fluctuates in time, mainly when the pulse is on (coin toss). Regular intervals of the pulse in (b) indicate the regular discrete time steps of the QW. The parameters used in our simulations are $\omega_q/2\pi = 7$ GHz, $D/2\pi = 2.87$ GHz, $\eta/2\pi = 100$ MHz, $\epsilon_0/2\pi = 1$ GHz, $\gamma_1/2\pi = 0.02$ MHz, $\gamma_\phi/2\pi = 0.31$ MHz, and $\Gamma/2\pi = 0.1$ MHz. The repetition rate of the driving pulsed laser is taken as $\omega_p = \chi d$, with $d = 16$ being the number of sites on the cycle of a QW.

As our improved procedure is general and applicable to previous circuit QED or cavity QED settings [131, 11], we shall first use the original values $\gamma_1/2\pi = 0.02$ MHz and $\epsilon_0/2\pi = 1$ GHz for comparison of our improved procedure with the original ones in Refs. [131, 11]. The minor difference of no consequence is that we use $D/2\pi = 2.87$ GHz [148] for the zero-field splitting between the $|\ m = 0\rangle$ and $|\ m = \pm 1\rangle$ ground state spin triplet levels of the NV center. This corresponds to cavity or transmission line mode frequency, which is taken as 5 MHz in Refs. [131, 11].

Following the comparison, we present the results for the actual flux qubit and NV ensemble parameters. Relaxation rate of the flux qubit is of the same order with its dephasing rate so that we set $\gamma_1/2\pi = 0.31$ MHz [172]. Longitudinal relaxation time T_1 of the NV center electron spin is in the order of few milliseconds at room

temperature [143] and gets longer by reducing the temperature. The dephasing time of the spin T_2 is in the order of $0.3-2$ ms and gets longer by increasing the purity of the diamond sample isotropically [173]. In the case of quasimagnons, the decoherence rate Γ would be collectively enhanced, similar to the collectively enhanced coupling strength. For $N = 3.1 \times 10^7$ and $T_2 = 2$ ms, we find $\Gamma/2\pi = 2.78$ which is larger than the circuit QED and cavity QED cases where $\Gamma/2\pi = 0.1$ MHz [131, 11]. To compensate it we take larger drive strength $\epsilon_0/2\pi = 10$ GHz.

Relative to the decoherence [174] and dephasing [175] of the qubit, as well as to the relaxation of the NV centers, the system is in the strong-coupling regime, though still not in the ultrastrong-coupling regime, which would challenge the validity of rotating wave and Born-Markov approximations.

The repetition rate of the driving pulsed laser is taken to be $\omega_p = \chi d$, with $d = 16$ being the number of sites on the cycle of a QW. This yields the duration of each time step of the QW as $t_p = 2\pi/\omega_p$. This time covers the pulse duration of $t_H = \pi/(\sqrt{2}\Omega_{R0})$ with $\Omega_{R0} := 2\pi\epsilon_0/\Delta$ as well as the time between pulses. Hadamard coin operation induced by the pulse can be described by the Hamiltonian

$$H_{\text{coin}} = \frac{\Omega_R}{2}(\sigma_x + \sigma_z), \tag{4.26}$$

if we take the operation time as t_H; and if we decouple the quasi-magnon dynamics from the qubit dynamics. For that aim, let us drop the constant term $(\chi/2)1_2$ and rewrite the effective QW Hamiltonian in Eq. (4.21) as

$$H_{\text{eff}} = H_{\text{coin}} + (\chi c^\dagger c - \bar{n})\sigma_z - \delta_c c^\dagger c + \epsilon(c + c^\dagger), \tag{4.27}$$

under the condition of

$$\chi\bar{n} - \frac{\delta_d}{2} + \frac{\chi}{2} = \frac{\Omega_R}{2}. \tag{4.28}$$

This condition can be satisfied by taking the pulse frequency to be

$$\omega_d = (2\bar{n} + 1)\chi + \omega_q - \Omega_R, \tag{4.29}$$

where $\bar{n} = |\alpha|^2$ is the initial number of quasi-magnons. ϵ_0 is the amplitude of the square pulse. If the number fluctuations are sufficiently small, then the dynamics of the quasi-magnons are uncoupled from the qubit degrees of freedom, whose evolution would be a faithful representation of that of an ideal Hadamard coin. Quantitatively, if we denote the number fluctuations by δn, the condition of validity can be expressed as $\chi\delta n \ll \Omega_R/2$ or $\delta n \ll \epsilon_0/\eta$, which becomes $\delta n \ll 10 - 100$ for our parameters. Our simulations indicate that number fluctuations remain in the order of few quasi-magnons; and thus the coin operation can be simulated. In contrast to the cirQED and CQED QW proposals, we do not change ω_d by changing $\bar{n}$ at every step. Furthermore, the pulse duration, and hence, the time steps, are fixed in our approach. These two differences allow for simpler implementation as well as for direct interpretation in terms of DTQW with regular time steps.

We first examine the behavior of the number of quasimagnons, $\langle n_c \rangle = \langle c^\dagger c \rangle$, and the qubit excited and ground level populations, which are respectively defined to be $P_e = (1 + \langle \sigma_z \rangle)/2$, and $P_g = (1 - \langle \sigma_z \rangle)/2$. Their time evolutions are shown in Fig. 4-2. The initial number of quasimagnons is $n_c(0) = 9$. Fig. 4-2(a) indicates that during the course of dynamics mean number of quasimagnons fluctuates because of the drive and dissipation. Relatively Strong fluctuations in the mean quasimagnon number occur mainly when the pulse is on, or when the Hadamard coin is tossed. When the pulse is off, a conditional phase shift operation characterized by the parameter χ is set into action. During this rotational QW step in quasimagnon phase space, fluctuations of the $\langle n_c \rangle$ are much smaller. The dynamics of the coin, or the populations of the qubit levels, can be followed by the Fig. 4-2(b). We have marked the regions during which the pulse is on. The dynamics and exchanges between the upper and lower level populations reveal that the qubit evolves in close correlation with the simulation of a pure Hadamard coin. Exchanges only occur when the pulse is on, or at the end of

the coin toss.

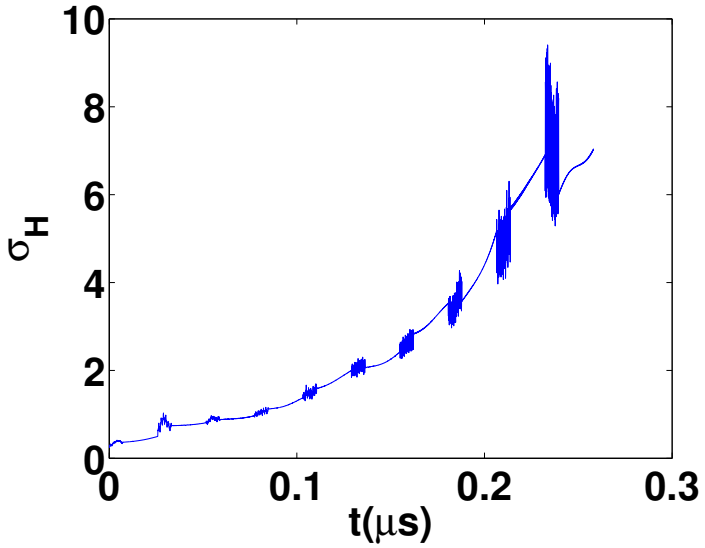

Figure 4-3: Time (t) dependence of the Holevo standard deviation measure $\sigma_{\rm H}$ in the system for the initial state $|\psi(0)\rangle = |\alpha = 3\rangle(|g\rangle + i|e\rangle)/\sqrt{2}$. Its decrease beyond the seventh step is due to the cyclic wrapping-up effect in terms of the definition of the Holevo measure; it does not represent the actual behavior of the QW. The parameters are the same as Fig. 4-2.

QW in the quasimagnon phase space needs to be characterized by examination of the dispersion of the angular variable ϕ. For cyclic variables the variance is conveniently determined by the Holevo standard deviation which is defined as [176]

$$\sigma_{\rm H} = \sqrt{|\langle {\rm e}^{{\rm i}\phi}\rangle|^{-2} - 1}, \tag{4.30}$$

where

$$\left|\langle {\rm e}^{{\rm i}\phi}\rangle\right| = \left|\int_{-\pi}^{\pi} {\rm d}\phi P(\phi){\rm e}^{{\rm i}\phi}\right| \tag{4.31}$$

is the *sharpness* of the phase distribution. Sharpness is bounded between 0, for spiked distribution at the mean phase, and 1, for a flat distribution. It can be interpreted as the success or fidelity of the phase distribution to estimate the mean phase [177, 178]. Here we take the mean phase as 0 and choose the domain as $[-\pi, \pi]$. The phase

distribution $P(\phi)$ is determined from the reduced density matrix of the quasimagnons $\rho_{\rm m}$ by using

$$P(\phi) = \lim_{M\to\infty} \langle \phi \mid \rho_{\rm m} \mid \phi \rangle, \tag{4.32}$$

where the phase states $|\phi\rangle$ in an M-dimensional Fock space are defined in Eq. (4.23). The quasimagnon reduced density matrix is calculated by, $\rho_{\rm m} = {\rm Tr_q}(\rho)$, taking the trace over the qubit degrees of freedom of the density matrix of the system ρ, which is found by solving Eq. (4.24). If the phase variance $(\Delta\phi)^2 = \langle\phi^2\rangle - \langle\phi\rangle^2$ is small ($(\Delta\phi)^2 \ll 1$) then $\sigma_{\rm H}$ becomes equivalent to the $\Delta\phi$. In contrast to localized distributions, Holevo variance is infinitely large for flat distributions with zero sharpness. In our case, this situation corresponds to large phase diffusion due to decoherence in the system. We examine the Wigner function evolution to determine the number of steps for which the Holevo measure can be used for reliable information on the phase variance.

Fig. 4-3 shows that $\sigma_{\rm H}$ increases in an almost smooth manner during the conditional phase shifts, whereas during the coin toss operation, it shows rapid oscillations. At the eighth step, more than half of the cycle is covered by the Wigner function (see Fig. 4-6). The Holevo measure becomes unsuitable for describing the second order phase variance beyond this point. Similar behavior is encountered in the cirQED QW proposal [11]. To check whether the phase variance is faster than that of the classical random walk, we employ a linear fit analysis for the first 7 steps using MATLAB. The result is shown in Fig. 4-4. The upper panel in Fig. 4-4 reveals that there is a linear relation between the number of regular time steps and the logarithm of the Holevo standard deviation. The slope is determined to be $\sim 0.96 \pm 0.11$, where 0.11 is the linear-regression standard deviation. This result is close enough to the ballistic case to declare it to be ballistic given that phase diffusion due to decoherence and wrapping due to periodicity of phase have occured. In the case of the classical random walk, the slope would be 0.5.

The observation of further QW signatures is to be expected, similar to earlier

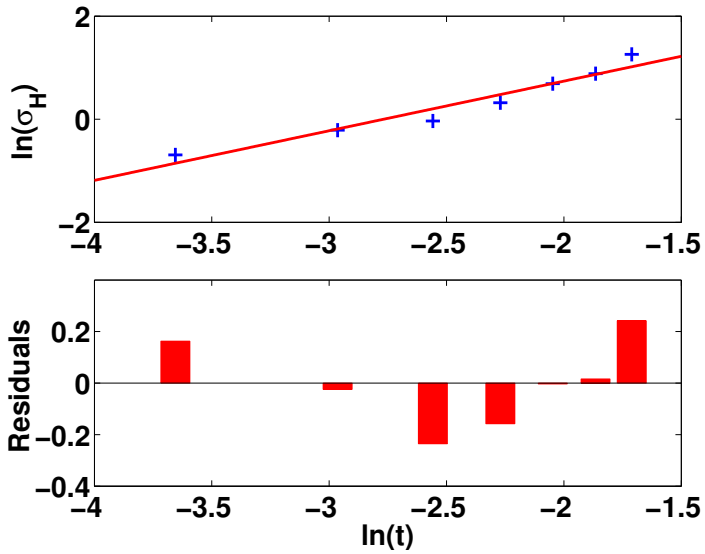

Figure 4-4: A linear fit to the Holevo measure $\sigma_{\rm H}$ in Fig. 4-3. A logarithmic scale is used for both axes. The initial starting point in time is taken as zero and not used on the logarithmic scale. The slope of the line is calculated as $\sim$0.96, which is in the ballistic regime and higher than the corresponding value of 0.5 for a classical random walk. The parameters are the same as Fig. 4-2, except that the time t here is dimensionless, scaled by 1 μs.

studies on the same Hamiltonian for similar parameters. For example, the phase distributions at the end of the first four steps are reported in Ref. [11]. Interpretation of the phase distribution is not trivial because of the effects of the pump field. It is found that as the pump intensity grows, the distribution becomes asymmetrically skewed in one direction. Moreover, some peaks become narrower. We present the phase distribution in Fig. 4-5. We used $M = 256$ phase states in our numerical calculations. Phase distribution is skewed counterclockwise because of the pumping field, consistent with the observations reported in Ref. [11]. Because the walk occurs on a circle, the left and the right boundaries $\phi = \pm\pi$ in Fig. 4-5 are the same. The initial phase distribution of the QW starts at an angular location of $\phi = 0$. The spread of the distribution is quadratically enhanced, relative to that of a classical random walk.

Wigner functions at the end of the first eight steps are shown in Fig. 4-6. The spread along the angular direction as the QW progress is accompanied by the increas-

ing deformation along the radial direction due to the number fluctuations. QW splits into other circles at different mean number of quasimagnons and dephasing occurs. Holevo measure increases beyond 1 as the distribution gets more and more flat due to significant contribution of the phase diffusion after 7 steps. Thus we did not use the Holevo measure to characterize the QW for more than 7 steps.

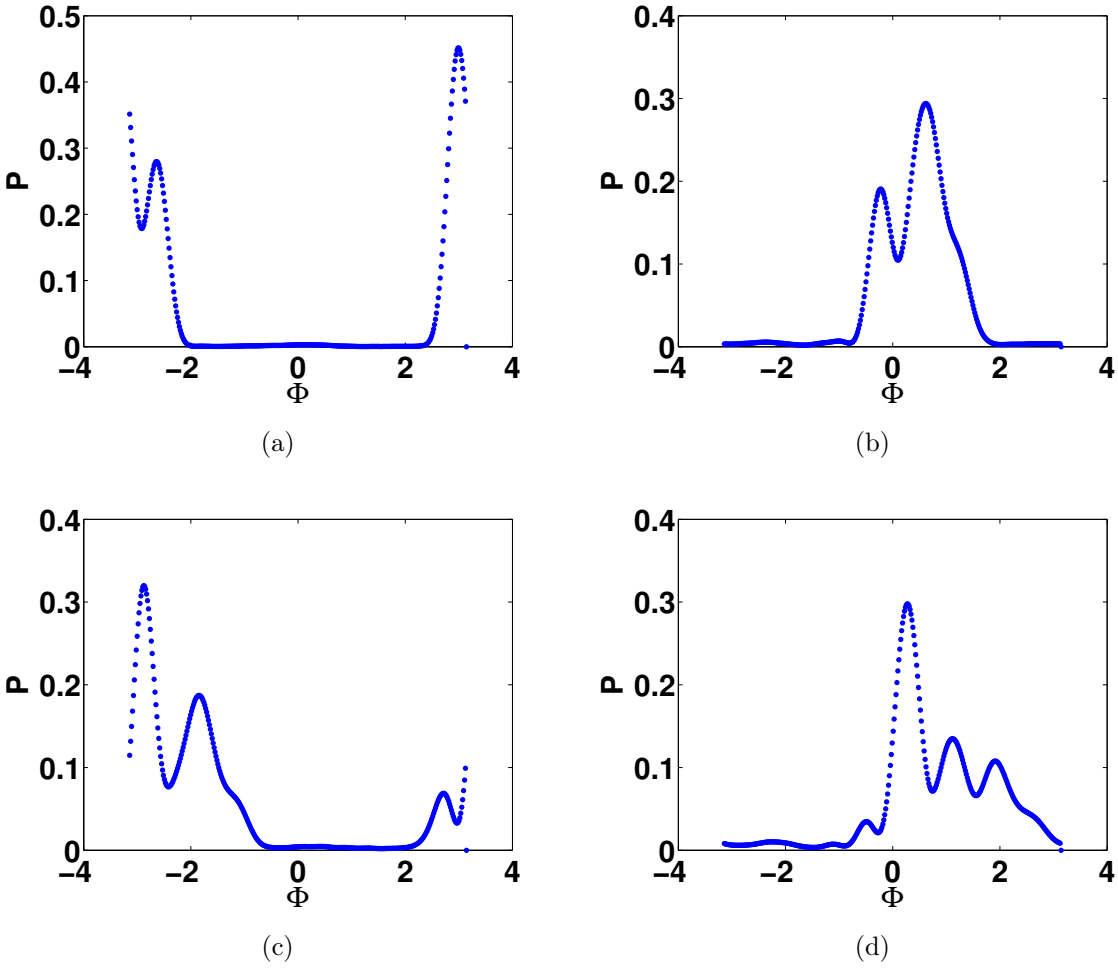

Figure 4-5: The phase distribution $P = P(\Phi)$ as a function of the angular variable Φ of the quasimagnon phase space is shown at the end of the (a) first, (b) second, (c) third, and the (d) fourth steps of the QW. The initial phase distribution, wherein the QW starts at $\Phi = 0$, is not shown. The parameters are the same as Fig. 4-2. Φ is in radians.

We now examine the effect of decoherence rate of presently available NV center ensembles with $\Gamma/2\pi = 2.78$ MHz [173] which is about 10 times larger than the photons in cirQED and CQED QW proposals. To compensate faster loss of quasi-

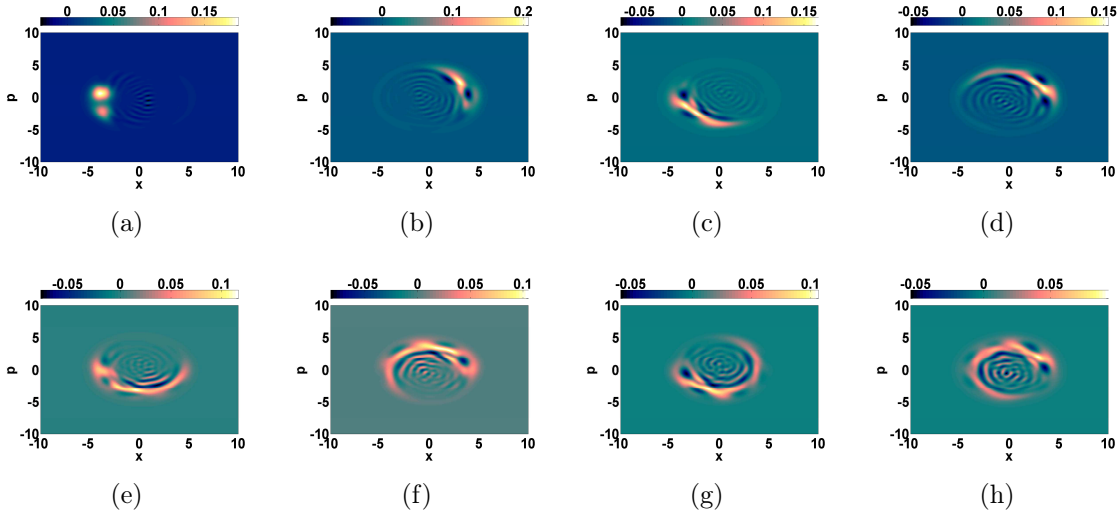

Figure 4-6: The Wigner function at the end of the first eight steps of the QW. The parameters are the same as Fig. 4-2. Real and imaginary parts of the coherent state parameter in the quasimagnon phase space are denoted by x and p, respectively. The initial Wigner function, which is a Gaussian centered at $(x = 3, p = 0)$, is not shown. The radius of the circle of the QW is determined by the square root of the mean number of the quasimagnons. Phase diffusion along the angular direction is accompanied by the ripples along the radial direction due to the number fluctuations as the QW progress.

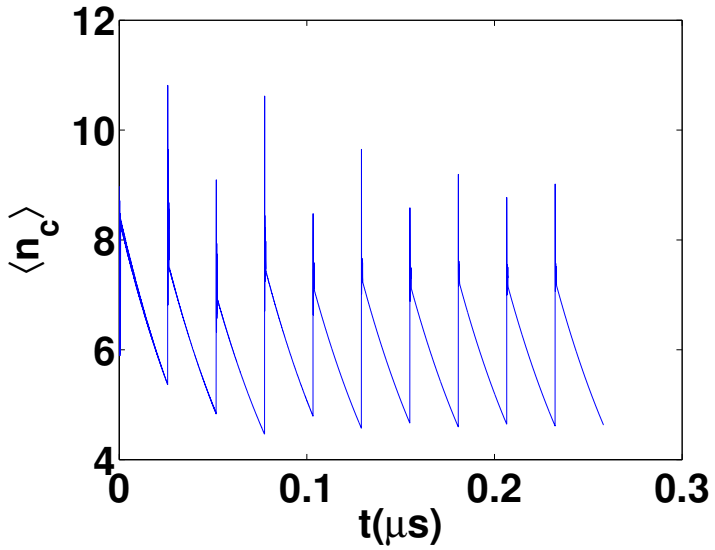

Figure 4-7: Time (t) dependence of the mean quasimagnon number $\langle n_c \rangle$ under the same conditions as in Fig. 4-2 but for the case of $\Gamma/2\pi = 2.78$ MHz and drive $\epsilon_0/2\pi = 10$ GHz.

magnons, we take 10 times stronger drive with $\epsilon_0/2\pi = 10$ GHz in the simulations, which is found to be sufficient enough to stabilize the circular trajectory of quantum walkers in the phase space by maintaining $\langle n_c \rangle \sim 6$ as can be seen in Fig. 4-7. For this drive strength, the drive duration becomes 10 times shorter, due to the relation $t_H \sim 1/\Omega_R \sim 1/\epsilon_0$. The spikes in the figure correspond to the times when the drive is on or the action of coin toss. The Holevo standard deviation shown in the Fig. 4-8. In this case phase diffusion becomes significant after four steps. When we determine the linear fit in logarithmic scale we find the similar behavior as in Fig. 4-4 with the slope 0.98 ± 0.42, where 0.42 is the linear-regression standard deviation for the first four steps. Such a few number of steps yields large linear-regression standard deviation error in the slope. The slope is nevertheless close enough to be declared to be ballistic, given that phase diffusion due to significantly large decoherence and wrapping due to periodicity of phase have occured.

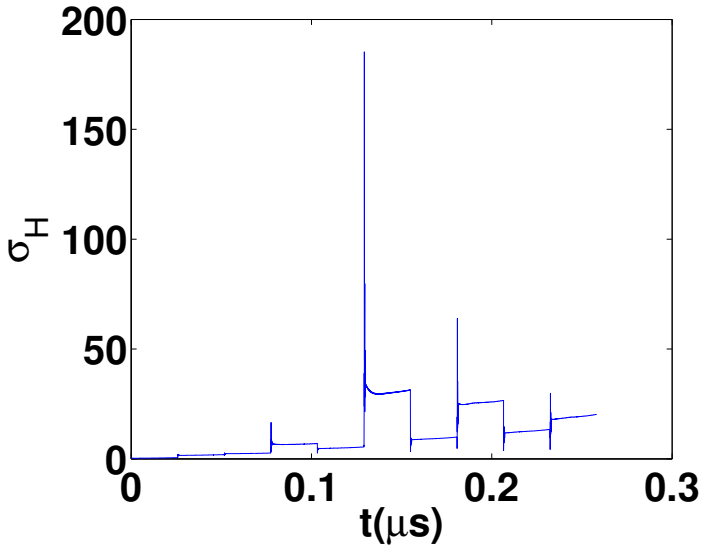

Figure 4-8: Time (t) dependence of the Holevo standard deviation measure σ_{H} under the same conditions as in Fig. 4-3 but for the case of $\Gamma/2\pi = 2.78$ MHz and drive $\epsilon_0/2\pi = 10$ GHz.

4.3 Appendix

4.3.1 Hubbard, Schwinger and Quasimagnon Operators

Here we summarize the algebraic properties and relations among the Hubbard operators, bilinear Schwinger boson forms and the quasimagnon operators. For notational simplicity we drop the NV center crystallographic class index f. Let us introduce the Gell-mann isotopic spin representation of SU(3) [179] in terms of the Hubbard operators,

$$V_- = \frac{X^{0-}}{\sqrt{N}}, \quad U_- = \frac{X^{0+}}{\sqrt{N}}, \quad T_- = X^{-+}, \tag{4.33}$$

$$V_3 = \frac{X^{--} - X^{00}}{2N}, \quad U_3 = \frac{X^{++} - X^{00}}{2N}, \tag{4.34}$$

$$T_3 = \frac{X^{++} - X^{--}}{2}, \tag{4.35}$$

with $V_+ = V_-^\dagger, U_+ = U_-^\dagger$ and $T_+ = T_-^\dagger$. Each U, V, T spin-1/2 subgroup obeys SU(2) algebra, $[J_-, J_+] = -2J_3$, $[J_3, J_\pm] = \pm J_\pm$ with $J = U, V, T$; but they are all correlated according to the full set of commutation relations of the Lie algebra of SU(3).

SU(3) commutation relations can be obtained using the Hubbard operator algebra

$$[X^{mn}, X^{m'n'}] = \delta_{m'n} X^{mn'} - \delta_{mn'} X^{m'n}, \tag{4.36}$$

which is preserved under the bilinear Schwinger map $X^{mn} = x_m^\dagger x_n$. We associate the collective spin Hubbard operators introduced for the NV center spin ensemble with the Schwinger map subject to weak excitation condition relative to large N so that $x_0^\dagger x_0 \approx N \gg 1$. In particular the U and V spins become decoupled

$$[V_-, U_+] = -\frac{T_+}{N} \approx 0, \tag{4.37}$$

and contracted into Weyl-Heisenberg algebra according to

$$[V_-, V_+] = -2V_3 \approx 1. \tag{4.38}$$

The bosonization of the U and V spins in terms of the quasimagnon operators

$$V_- = \frac{X^{0-}}{\sqrt{N}} = \frac{x_0^\dagger x_-}{\sqrt{N}} \approx x_- \equiv b, \tag{4.39}$$

$$U_- = \frac{X^{0+}}{\sqrt{N}} = \frac{x_0^\dagger x_+}{\sqrt{N}} \approx x_+ \equiv a, \tag{4.40}$$

physically means that the particle label counting the individual (NV center) spins in the collective spin has lost its meaning for weak excitations in a large ensemble. This allows for quasimagnon description of weak excitations and spin liquid interpretation of NV center ensemble. Mathematicaly this construction is equivalent to contraction of $SU(3)$ into the semidirect product $SU(2)\bar{\otimes}h_2$ of T spin algebra, which remains unaffected by the bosonization condition, and quasimagnon Weyl-Heisenberg algebra [180].

4.3.2 Coupled and Uncoupled Quasimagnon Modes with a Flux Qubit

Two quasimagnon modes corresponding to two quasispin waves with different polarizations are nearly degenerate. This allows for decoupling a combination of them from the flux qubit. The annihilation operators for the coupled and uncoupled modes are $c_f = (a_f + b_f)/\sqrt{2}$ and $d_f = (a_f - b_f)/\sqrt{2}$, respectively. These are also nearly degenerate, whereby subsequent decouplings are possible. New annihilation operators, given by

$$\begin{aligned}
c_{12} &= \frac{1}{\sqrt{N_1 + N_2}}(\sqrt{N_1}c_1 + \sqrt{N_2}c_2), \\
d_{12} &= \frac{1}{\sqrt{N_1 + N_2}}(\sqrt{N_2}c_1 - \sqrt{N_1}c_2), \\
c_{34} &= \frac{1}{\sqrt{N_3 + N_4}}(\sqrt{N_3}c_3 + \sqrt{N_4}c_4), \\
d_{34} &= \frac{1}{\sqrt{N_3 + N_4}}(\sqrt{N_4}c_3 - \sqrt{N_3}c_4),
\end{aligned} \tag{4.41}$$

are defined to decouple d_{12} and d_{34} from the qubit.

When the procedure is applied once more, it leads to the coupling of the qubit to a mode described by the annihilation operator

$$\begin{aligned} c &= \frac{\sqrt{N_1+N_2}c_{12}+\sqrt{N_3+N_4}c_{34}}{\sqrt{N}} \\ &= \frac{1}{\sqrt{2N}}(\sum_f \sqrt{N_f}(a_f+b_f), \end{aligned} \tag{4.42}$$

with $N=\sum_f N_f$ as the total number of NV^- centers. The uncoupled mode is given by

$$d=\frac{\sqrt{N_3+N_4}c_{12}-\sqrt{N_1+N_2}c_{34}}{\sqrt{N}}. \tag{4.43}$$

4.3.3 Inhomogeneous Coupling and Broadening of NV Centers

Our model was developed under the assumptions of spatially homogeneous coupling of the NV center ensemble to the flux qubit and absence of inhomogeneous broadening. Here we consider the more general case of spatial inhomogeneity for which the model Hamiltonian $H=H_{\rm NV}+H_q+H_{\rm int}$ should be generalized for the position dependent zero field splitting D_i and spatially inhomogeneous coupling g_i.

The NV center ensemble Hamiltonian becomes

$$H_{\rm NV}=\sum_{f=1}^{4}\sum_{i=1}^{N_f}\sum_{m=0,\pm1} D_i m^2 X_{fi}^{mm}, \tag{4.44}$$

where the Hubbard operators for each NV is defined to be

$$X_{fi}^{mm}=\mid m\rangle_i^{(f)}\langle m\mid_i^{(f)}. \tag{4.45}$$

For the single NV center the weak excitation condition can be used for introducing bilinear Schwinger map $X_{fi}^{mn}=x_{fim}^{\dagger}x_{fin}$ with $x_{fi0}\approx 1$. Using the notation $x_{fi+}\equiv a_{fi}$

and $x_{fi-} \equiv b_{fi}$, we write the $H_{\rm int}$ as

$$H_{\rm int} = \sum_{fi} g_i[\sigma_+(a_{fi} + b_{fi}) + \text{H.c.}]. \tag{4.46}$$

Introducing $c_{fi} = (a_{fi} + b_{fi})/\sqrt{2}$ and dropping the uncoupled mode $d_{fi} = (a_{fi} - b_{fi})/\sqrt{2}$, the Hamiltonian becomes a spin-boson model

$$H = \frac{\omega_q}{2} + \sum_{fi} D_i c_{fi}^\dagger c_{fi} + g_i(\sigma_+ c_{fi} + \text{H.c.}). \tag{4.47}$$

We can now identify the bosonic collective mode that is coupled to the flux qubit as

$$c = \frac{1}{G}\sum_f G_f c_f, \tag{4.48}$$

where

$$G_f = \sqrt{2\sum_i g_i^2}, \quad G = \sqrt{\sum_f G_f^2}, \tag{4.49}$$

and

$$c_f = \frac{1}{G_f}\sum_i g_i(a_{fi} + b_{fi}). \tag{4.50}$$

This shows that quasimagnon picture can be used in the presence of spatially dependent coupling; albeit the quasimagnon mode would be subject to dephasing effect of the inhomogeneous broadening.

The coupling $H_{\rm int} = G(\sigma_+ c + \text{H.c.})$ of the flux qubit and the quasimagnon mode leads to a qubit-polariton energy gap. This gap can protect the quasimagnon against dephasing if it is sufficiently strong. A more intriguing proposal would be to exploit a particular inhomogeneous coupling density profile $\rho(\omega)$ to optimize linewidth reduction [181]. This method has been suggested for cavity-spin ensemble coupling [181],

where it has been shown that a Gaussian coupling density profile reduce the polariton linewidth to a limit independent of inhomogeneous linewidth. In general, it has been found that the coupling density should fall off as $1/\omega^3$ or faster for the manifestation of the polariton gap induced line narrowing.

Another challenge for the experimental implementation of our model in the presence of spatial inhomogeneity would be to drive the exact quasimagnon mode. For spatially homogeneous case this mode is always accessed by the drive. If the drive field spatial profile can be adjusted to match with the magnetic field profile of the flux qubit that couples to the NV center ensemble, then the quasimagnon mode in the spatial inhomogenity case can be driven as well.

Chapter 5

Concluding Remarks

In this thesis, we first examined a system of cavities, coupled with two-photon exchange interaction, from the perspective of dynamical transfer of particle entanglement between photonic and atomic subsystems. We considered ideal evolution of initially entangled and unentangled states without dissipation and used exact analytical solutions of the model system. Secondly, we addressed the quantum correlations in the stationary solutions of the master equation of a system of nonlinear coupled cavities by taking into account the open system conditions under drive and dissipation. Here, the subtle relations between delocalization and localization and the quantum coherence were examined from the point of view of quantum correlations.

Lastly, we proposed a fully solid-state implementation of a DTQW of NV centers in diamond coupled to a flux qubit. The QW takes place in the phase space of the quasimagnon field by indirectly flipping the flux-qubit coin. The proposed scheme is an improved version of the one originally developed for cirQED and cavity QED systems. In our method, the time steps are of fixed duration and no alteration of the pulse is required. This improved method is applicable to general cirQED and cavity QED QW scenarios.

Further studies may focused on merging these investigations all together. Our proposal for discrete-time quantum walks still suffers from phase diffusion and wrapping effects due to the decoherence and the periodicity of the phase, respectively. Therefore, the problem becomes finding a way to reduce quantum fluctuations in the

phase space of the quantum walker. To this end, we may consider nonlinear terms which can be added to the system Hamiltonian systematically to create squeezing. Alternatively, we may also consider initially (phase and amplitude) squeezed states of the quantum walker with keeping the Hamiltonian untouched. While the former may squeeze the quantum state of the walker in ever step during the time evolution, the latter, in particular the phase squeezed states, may also effectively reduce the fluctuations and increase the number of steps of the walker significantly.

We may extend our work to the case of two- or more quantum correlated walkers on the same cycle as well as on the same line. The walkers can share a single coin or each can have its own. In the latter case, by letting the walkers totally or partially swap the coins after each flip, quantum entanglement between position and coin degrees of freedom can be formed. More interestingly, such swapping of coins induces quantum correlations to the subsystem of the walkers that do not directly interact with each other. Unlike to the case of the classical random walk, where the state of the coin is insignificant for the dynamics of the walkers, here, we may able to examine the effects of the quantum correlations on the dynamics of the system.

Finally, simulation of DTQW on coupled cycles can be considered as well by letting the walker hop between two or more cycles. Distribution of the quantum states of the walker between different optical paths will lead to the path entanglement, a concept which is particularly important for quantum computation. Moreover, we can compare single walker path entangled case with the multi-walker correlated case and try to determine or model a system for quantum random walks which is more efficient and relatively easy to implement with the current CQED or cirQED technologies.

Bibliography

[1] I. I. Rabi. On the process of space quantization. *Phys. Rev.*, 49:324–328, Feb 1936.

[2] I. I. Rabi. Space quantization in a gyrating magnetic field. *Phys. Rev.*, 51:652–654, Apr 1937.

[3] E T. Jaynes and F. W. Cummings. Comparison of quantum and semiclassical radiation theories with application to the beam maser. *Proc. IEEE*, 51(1):89–109, 1963.

[4] M. O. Scully and M. S. Zubairy. *Quantum Optics*. Cambridge University Press, Cambridge, 1997.

[5] D. Braak. Integrability of the rabi model. *Phys. Rev. Lett.*, 107:100401, Aug 2011.

[6] Ze-Liang Xiang, Sahel Ashhab, JQ You, and Franco Nori. Hybrid quantum circuits: Superconducting circuits interacting with other quantum systems. *Reviews of Modern Physics*, 85(2):623, 2013.

[7] Brian David Josephson. Possible new effects in superconductive tunnelling. *Physics Letters*, 1(7):251–253, 1962.

[8] Yuriy Makhlin, Gerd Schön, and Alexander Shnirman. Quantum-state engineering with josephson-junction devices. *Reviews of modern physics*, 73(2):357, 2001.

[9] Salvador Elías Venegas-Andraca. Quantum walks: a comprehensive review. *Quantum Information Processing*, 11(5):1015–1106, 2012.

[10] Ben C Travaglione and Gerald J Milburn. Implementing the quantum random walk. *Physical Review A*, 65(3):032310, 2002.

[11] Peng Xue and Barry C. Sanders. Quantum quincunx for walk on circles in phase space with indirect coin flip. *New J. Phys.*, 10:053025, May 2008.

[12] Moorad Alexanian. Two-photon exchange between two three-level atoms in separate cavities. *Phys. Rev. A*, 83:023814, Feb 2011.

[13] S. Longhi. Optical realization of two-boson tunneling dynamics. *Physical Review A*, 83(4):43835, 2011.

[14] Xiang-Fa Zhou, Yong-Sheng Zhang, and Guang-Can Guo. Pair tunneling of bosonic atoms in an optical lattice. *Phys. Rev. A*, 80:013605, Jul 2009.

[15] Masahiro Kitagawa and Masahito Ueda. Squeezed spin states. *Phys. Rev. A*, 47:5138–5143, Jun 1993.

[16] A. Sørensen, L. M. Duan, J. I. Cirac, and P. Zoller. Many-particle entanglement with bose–einstein condensates. *Nature*, 409(6816):63–66, 2001.

[17] M. Hillery. An introduction to the quantum theory of nonlinear optics. *Acta Physica Slovaca. Reviews and Tutorials*, 59(1):1–80, 2009.

[18] F. DellâĂŹAnno, S. De Siena, and F. Illuminati. Multiphoton quantum optics and quantum state engineering. *Physics reports*, 428(2):53–168, 2006.

[19] Asoka Biswas and G. S. Agarwal. Transfer of an unknown quantum state, quantum networks, and memory. *Phys. Rev. A*, 70:022323, Aug 2004.

[20] J. I. Cirac, P. Zoller, H. J. Kimble, and H. Mabuchi. Quantum state transfer and entanglement distribution among distant nodes in a quantum network. *Phys. Rev. Lett.*, 78:3221–3224, Apr 1997.

[21] L. Vernac, M. Pinard, and E. Giacobino. Quantum state transfer from light beams to atomic ensembles. *Eur. Phys. J. D*, 17(1):125–136, 2001.

[22] J. Hald, J. L. Sørensen, C. Schori, and E. S. Polzik. Spin squeezed atoms: A macroscopic entangled ensemble created by light. *Phys. Rev. Lett.*, 83:1319–1322, Aug 1999.

[23] A. Kuzmich, Klaus Mølmer, and E. S. Polzik. Spin squeezing in an ensemble of atoms illuminated with squeezed light. *Phys. Rev. Lett.*, 79:4782–4785, Dec 1997.

[24] Arup Banerjee. Generation of atomic-squeezed states in an optical cavity with an injected squeezed vacuum. *Phys. Rev. A*, 54:5327–5333, Dec 1996.

[25] Géza Tóth, Christian Knapp, Otfried Gühne, and Hans J. Briegel. Optimal spin squeezing inequalities detect bound entanglement in spin models. *Phys. Rev. Lett.*, 99:250405, Dec 2007.

[26] J. Ma, X. Wang, CP Sun, and F. Nori. Quantum spin squeezing. *Physics Reports*, 2011.

[27] M.O.T. Cunha, J.A. Dunningham, and V. Vedral. Entanglement in single-particle systems. *Proceedings of the Royal Society A: Mathematical, Physical and Engineering Science*, 463(2085):2277, 2007.

[28] SJ Van Enk. Single-particle entanglement. *Physical Review A*, 72(6):64306, 2005.

[29] F. Benatti, R. Floreanini, and U. Marzolino. Entanglement and squeezing with identical particles: ultracold atom quantum metrology. *Journal of Physics B: Atomic, Molecular and Optical Physics*, 44:091001, 2011.

[30] B. Öztop, M. Ö. Oktel, Ö. E. Müstecaplıoğlu, and L. You. Quantum entanglement of spin-1 bosons with coupled ground states in optical lattices. *J. Phys. B*, 42:145505, 2009.

[31] G. Tóth, C. Knapp, O. Gühne, and H.J. Briegel. Spin squeezing and entanglement. *Physical Review A*, 79(4):042334, 2009.

[32] Julien Vidal. Concurrence in collective models. *Phys. Rev. A*, 73:062318, Jun 2006.

[33] Giuseppe Vitagliano, Philipp Hyllus, Iñigo L. Egusquiza, and Géza Tóth. Spin squeezing inequalities for arbitrary spin. *Phys. Rev. Lett.*, 107:240502, Dec 2011.

[34] Y. Wu and X. Yang. Effective two-level model for a three-level atom in the xi configuration. *Physical Review A*, 56:2443–2446, 1997.

[35] Y. Wu. Effective raman theory for a three-level atom in the λ configuration. *Physical Review A*, 54(2):1586, 1996.

[36] Moorad Alexanian and Subir K. Bose. Unitary transformation and the dynamics of a three-level atom interacting with two quantized field modes. *Phys. Rev. A*, 52:2218–2224, Sep 1995.

[37] M. Alexanian, S. Bose, and L. Chow. Trapping and fock state generation in a two-photon micromaser. *J. Mod. Opt.*, 45(12):2519–2532, 1998.

[38] Julien Vidal, Guillaume Palacios, and Claude Aslangul. Entanglement dynamics in the lipkin-meshkov-glick model. *Phys. Rev. A*, 70:062304, Dec 2004.

[39] Pedro Ribeiro, Julien Vidal, and Rémy Mosseri. Exact spectrum of the lipkin-meshkov-glick model in the thermodynamic limit and finite-size corrections. *Phys. Rev. E*, 78:021106, Aug 2008.

[40] Pedro Ribeiro, Julien Vidal, and Rémy Mosseri. Thermodynamical limit of the lipkin-meshkov-glick model. *Phys. Rev. Lett.*, 99:050402, Aug 2007.

[41] V.P. Karassiov and A.B. Klimov. An algebraic approach to solving evolution problems in some nonlinear quantum models. *Physics Letters A*, 189(1-2):43–51, 1994.

[42] P.W. Higgs. Dynamical symmetries in a spherical geometry. i. *Journal of Physics A: Mathematical and General*, 12:309, 1979.

[43] H. J. Carmichael. Quantum fluctuations in absorptive bistability without adiabatic elimination. *Phys. Rev. A*, 33:3262–3269, May 1986.

[44] M. Alexanian. Scattering of two coherent photons inside a one-dimensional coupled-resonator waveguide. *Physical Review A*, 81(1):015805, 2010.

[45] JA Schreier, AA Houck, J. Koch, DI Schuster, BR Johnson, JM Chow, JM Gambetta, J. Majer, L. Frunzio, MH Devoret, et al. Suppressing charge noise decoherence in superconducting charge qubits. *Physical Review B*, 77(18):180502, 2008.

[46] C.P. Yang. Fast quantum information transfer with superconducting flux qubits coupled to a cavity. *Journal of Physics A: Mathematical and Theoretical*, 45(20):205304, 2012.

[47] D. Petrosyan, G. Bensky, G. Kurizki, I. Mazets, J. Majer, and J. Schmiedmayer. Reversible state transfer between superconducting qubits and atomic ensembles. *Physical Review A*, 79(4):040304, 2009.

[48] P. Forn-Díaz, J. Lisenfeld, D. Marcos, J. J. García-Ripoll, E. Solano, C. J. P. M. Harmans, and J. E. Mooij. Observation of the bloch-siegert shift in a qubit-oscillator system in the ultrastrong coupling regime. *Phys. Rev. Lett.*, 105:237001, Nov 2010.

[49] J. Casanova, G. Romero, I. Lizuain, J. J. García-Ripoll, and E. Solano. Deep strong coupling regime of the jaynes-cummings model. *Phys. Rev. Lett.*, 105:263603, Dec 2010.

[50] M. Hofheinz, EM Weig, M. Ansmann, R.C. Bialczak, E. Lucero, M. Neeley, AD OâĂŹConnell, H. Wang, J.M. Martinis, and AN Cleland. Generation of fock states in a superconducting quantum circuit. *Nature*, 454(7202):310–314, 2008.

[51] D. Bozyigit, C. Lang, L. Steffen, JM Fink, C. Eichler, M. Baur, R. Bianchetti, PJ Leek, S. Filipp, MP da Silva, et al. Antibunching of microwave-frequency photons observed in correlation measurements using linear detectors. *Nature Physics*, 7(2):154–158, 2010.

[52] B. S. Ham and P. R. Hemmer. Coherence switching in a four-level system: quantum switching. *Phys. Rev. Lett.*, 84(18):4080–4083, 2000.

[53] M. A. Nielsen and I. L. Chuang. *Quantum Computation and Quantum Information*. Cambridge university press, 2010.

[54] G. Vidal, J. I. Latorre, E. Rico, and A. Kitaev. Entanglement in quantum critical phenomena. *Phys. Rev. Lett.*, 90(22):227902, 2003.

[55] SL Sondhi, SM Girvin, JP Carini, and D. Shahar. Continuous quantum phase transitions. *Rev. Mod. Phys.*, 69(1):315, 1997.

[56] M. Schiró, M. Bordyuh, B. Öztop, and H. E. Türeci. Phase transition of light in cavity qed lattices. *Phys. Rev. Lett.*, 109:053601, Aug 2012.

[57] Dimitris G. Angelakis, Marcelo Franca Santos, and Sougato Bose. Photon-blockade-induced mott transitions and xy spin models in coupled cavity arrays. *Phys. Rev. A*, 76:031805, Sep 2007.

[58] Davide Rossini and Rosario Fazio. Mott-insulating and glassy phases of polaritons in 1d arrays of coupled cavities. *Phys. Rev. Lett.*, 99:186401, Oct 2007.

[59] Markus Aichhorn, Martin Hohenadler, Charles Tahan, and Peter B. Littlewood. Quantum fluctuations, temperature, and detuning effects in solid-light systems. *Phys. Rev. Lett.*, 100:216401, May 2008.

[60] Neil Na, Shoko Utsunomiya, Lin Tian, and Yoshihisa Yamamoto. Strongly correlated polaritons in a two-dimensional array of photonic crystal microcavities. *Phys. Rev. A*, 77:031803, Mar 2008.

[61] S. Schmidt and G. Blatter. Strong coupling theory for the jaynes-cummings-hubbard model. *Phys. Rev. Lett.*, 103:086403, Aug 2009.

[62] Jens Koch and Karyn Le Hur. Superfluid–mott-insulator transition of light in the jaynes-cummings lattice. *Phys. Rev. A*, 80:023811, Aug 2009.

[63] Peter Pippan, Hans Gerd Evertz, and Martin Hohenadler. Excitation spectra of strongly correlated lattice bosons and polaritons. *Phys. Rev. A*, 80:033612, Sep 2009.

[64] A. Tomadin, V. Giovannetti, R. Fazio, D. Gerace, I. Carusotto, H. E. Türeci, and A. Imamoglu. Signatures of the superfluid-insulator phase transition in laser-driven dissipative nonlinear cavity arrays. *Phys. Rev. A*, 81:061801, Jun 2010.

[65] S. Schmidt and G. Blatter. Excitations of strongly correlated lattice polaritons. *Phys. Rev. Lett.*, 104:216402, May 2010.

[66] Michael J Hartmann, Fernando GSL Brandão, and Martin B Plenio. Strongly interacting polaritons in coupled arrays of cavities. *Nature Physics*, 2(12):849–855, 2006.

[67] Andrew D Greentree, Charles Tahan, Jared H Cole, and Lloyd CL Hollenberg. Quantum phase transitions of light. *Nature Physics*, 2(12):856–861, 2006.

[68] S. Saito, M. Thorwart, H. Tanaka, M. Ueda, H. Nakano, K. Semba, and H. Takayanagi. Multiphoton transitions in a macroscopic quantum two-state system. *Phys. Rev. Lett.*, 93:037001, Jul 2004.

[69] S. Ferretti, L. C. Andreani, H. E. Türeci, and D. Gerace. Photon correlations in a two-site nonlinear cavity system under coherent drive and dissipation. *Phys. Rev. A*, 82(1):013841, 2010.

[70] H. Paul. Photon antibunching. *Rev. Mod. Phys.*, 54(4):1061, 1982.

[71] R. Horodecki, P. Horodecki, M. Horodecki, and K. Horodecki. Quantum entanglement. *Rev. Mod. Phys.*, 81(2):865, 2009.

[72] Moorad Alexanian. Two-photon exchange between two three-level atoms in separate cavities. *Physical Review A*, 83(2):023814, 2011.

[73] A. Ü. C. Hardal and Ö. E. Müstecaplıoğlu. Transfer of spin squeezing and particle entanglement between atoms and photons in coupled cavities via two-photon exchange. *J. Opt. Soc. Am. B*, 29(7):1822–1828, Jul 2012.

[74] Yu-Li Dong, Shi-Qun Zhu, and Wen-Long You. Quantum-state transmission in a cavity array via two-photon exchange. *Phys. Rev. A*, 85:023833, Feb 2012.

[75] Lev S. Bishop, Eran Ginossar, and S. M. Girvin. Response of the strongly driven jaynes-cummings oscillator. *Phys. Rev. Lett.*, 105:100505, Sep 2010.

[76] L. Tian and H. J. Carmichael. Quantum trajectory simulations of two-state behavior in an optical cavity containing one atom. *Phys. Rev. A*, 46:R6801–R6804, Dec 1992.

[77] P. J. Leek, S. Filipp, P. Maurer, M. Baur, R. Bianchetti, J. M. Fink, M. Göppl, L. Steffen, and A. Wallraff. Using sideband transitions for two-qubit operations in superconducting circuits. *Phys. Rev. B*, 79:180511, May 2009.

[78] J. A. Schreier, A. A. Houck, J. Koch, D. I. Schuster, B. R. Johnson, J. M. Chow, J. M. Gambetta, J. Majer, L. Frunzio, M. H. Devoret, S. M. Girvin, and R. J. Schoelkopf. Suppressing charge noise decoherence in superconducting charge qubits. *Phys. Rev. B*, 77:180502, May 2008.

[79] T. Niemczyk, F. Deppe, EP Menzel, MJ Schwarz, H. Huebl, F. Hocke, M. Häberlein, M. Danner, E. Hoffmann, A. Baust, et al. Selection rules in a strongly coupled qubit-resonator system. *arXiv:1107.0810*, 2011.

[80] F. Deppe, M. Mariantoni, EP Menzel, A. Marx, S. Saito, K. Kakuyanagi, H. Tanaka, T. Meno, K. Semba, H. Takayanagi, et al. Two-photon probe of the jaynes–cummings model and controlled symmetry breaking in circuit qed. *Nature Physics*, 4(9):686–691, 2008.

[81] M. Mariantoni, H. Wang, R. C. Bialczak, M. Lenander, E. Lucero, M. Neeley, AD OíConnell, D. Sank, M. Weides, J. Wenner, et al. Photon shell game in three-resonator circuit quantum electrodynamics. *Nature Physics*, 7(4):287–293, 2011.

[82] M. A. Marchiolli, D. Galetti, and T. Debarba. Spin squeezing and entanglement via finite-dimensional discrete phase-space description. *International Journal of Quantum Information*, 11(0):1330001, 2013.

[83] Xiaoguang Wang and Barry C. Sanders. Spin squeezing and pairwise entanglement for symmetric multiqubit states. *Physical Review A*, 68(1):012101, July 2003.

[84] Yan Dong, Wang Xiao-Guang, and Wu Ling-An. Spin squeezing and entanglement of many-particle spin-half states. *Chinese Physics Letters*, 22(2):271, February 2005.

[85] Ö. E. Müstecaplıoğlu. Quantum coherence and correlations of optical radiation by atomic ensembles interacting with a two-level atom in a microwave cavity. *Phys. Rev. A*, 83:023805, Feb 2011.

[86] H.J. Lipkin, N. Meshkov, and AJ Glick. Validity of many-body approximation methods for a solvable model::(i). exact solutions and perturbation theory. *Nuclear Physics*, 62(2):188–198, 1965.

[87] Pranaw Rungta, V. Bužek, Carlton M. Caves, M. Hillery, and G. J. Milburn. Universal state inversion and concurrence in arbitrary dimensions. *Phys. Rev. A*, 64:042315, Sep 2001.

[88] Mark Hillery and M. Suhail Zubairy. Entanglement conditions for two-mode states. *Phys. Rev. Lett.*, 96:050503, Feb 2006.

[89] Mark Hillery and M. Suhail Zubairy. Entanglement conditions for two-mode states: Applications. *Phys. Rev. A*, 74:032333, Sep 2006.

[90] S. J. van Enk. Single-particle entanglement. *Phys. Rev. A*, 72:064306, Dec 2005.

[91] R. Prevedel, G. Cronenberg, MS Tame, M. Paternostro, P. Walther, MS Kim, and A. Zeilinger. Experimental realization of dicke states of up to six qubits for multiparty quantum networking. *Phys. Rev. Lett.*, 103(2):20503, 2009.

[92] J. T. Barreiro, P. Schindler, O. Gühne, T. Monz, M. Chwalla, C. F. Roos, M. Hennrich, and R. Blatt. Experimental multiparticle entanglement dynamics induced by decoherence. *Nature Physics*, 6(12):943–946, 2010.

[93] JK Korbicz, O. Gühne, M. Lewenstein, H. Häffner, CF Roos, and R. Blatt. Generalized spin-squeezing inequalities in n-qubit systems: Theory and experiment. *Phys. Rev. A*, 74(5):052319, 2006.

[94] Michael J Hartmann, Fernando GSL Brandao, and Martin B Plenio. Quantum many-body phenomena in coupled cavity arrays. *Laser & Photonics Reviews*, 2(6):527–556, 2008.

[95] TCH Liew and V Savona. Quantum entanglement in nanocavity arrays. *Physical Review A*, 85(5):050301, 2012.

[96] X.F. Zhou, Y.S. Zhang, and G.C. Guo. Pair tunneling of bosonic atoms in an optical lattice. *Physical Review A*, 80(1):013605, 2009.

[97] D. S. Hall, M. R. Matthews, J. R. Ensher, C. E. Wieman, and E. A. Cornell. Dynamics of component separation in a binary mixture of bose-einstein condensates. *Phys. Rev. Lett.*, 81:1539–1542, Aug 1998.

[98] D. S. Hall, M. R. Matthews, C. E. Wieman, and E. A. Cornell. Measurements of relative phase in two-component bose-einstein condensates. *Phys. Rev. Lett.*, 81:1543–1546, Aug 1998.

[99] B. V. Hall, S. Whitlock, R. Anderson, P. Hannaford, and A. I. Sidorov. Condensate splitting in an asymmetric double well for atom chip based sensors. *Phys. Rev. Lett.*, 98:030402, Jan 2007.

[100] J Stenger, S Inouye, DM Stamper-Kurn, HJ Miesner, AP Chikkatur, and W Ketterle. Spin domains in ground-state bose-einstein condensates. *NATURE*, 396(6709):345–348, NOV 1998.

[101] Joanna Pietraszewicz, Tomasz Sowiński, Mirosław Brewczyk, Jakub Zakrzewski, Maciej Lewenstein, and Mariusz Gajda. Two-component bose-hubbard model with higher-angular-momentum states. *Physical Review A*, 85(5):053638, 2012.

[102] Jiasen Jin, Davide Rossini, Rosario Fazio, Martin Leib, and Michael J Hartmann. Photon solid phases in driven arrays of nonlinearly coupled cavities. *Physical review letters*, 110(16):163605, 2013.

[103] Maxime Boissonneault, Jay M Gambetta, and Alexandre Blais. Dispersive regime of circuit qed: Photon-dependent qubit dephasing and relaxation rates. *Physical Review A*, 79(1):013819, 2009.

[104] J.R. Johansson, P.D. Nation, and Franco Nori. QuTiP 2: A python framework for the dynamics of open quantum systems. *Computer Physics Communications*, 184(4):1234–1240, April 2013.

[105] Y. Kubo, F. R. Ong, P. Bertet, D. Vion, V. Jacques, D. Zheng, A. Dréau, J.-F. Roch, A. Auffeves, F. Jelezko, J. Wrachtrup, M. F. Barthe, P. Bergonzo, and D. Esteve. Strong coupling of a spin ensemble to a superconducting resonator. *Phys. Rev. Lett.*, 105:140502, Sep 2010.

[106] Alexandre Blais, Jay Gambetta, A. Wallraff, D. I. Schuster, S. M. Girvin, M. H. Devoret, and R. J. Schoelkopf. Quantum-information processing with circuit quantum electrodynamics. *Phys. Rev. A*, 75:032329, Mar 2007.

[107] Julien Vidal. Concurrence in collective models. *Physical Review A*, 73(6):062318, 2006.

[108] Biswajit Sen, Sandip Kumar Giri, Swapan Mandal, C. H. Raymond Ooi, and Anirban Pathak. Intermodal entanglement in raman processes. *Phys. Rev. A*, 87:022325, Feb 2013.

[109] Guifre Vidal and Reinhard F Werner. Computable measure of entanglement. *Physical Review A*, 65(3):032314, 2002.

[110] Martin B Plenio. Logarithmic negativity: A full entanglement monotone that is not convex. *Physical review letters*, 95(9):090503, 2005.

[111] Seth Lloyd. Hybrid quantum computing. *arXiv:quant-ph/0008057*, August 2000.

[112] C. Simon, M. Afzelius, J. Appel, A. Boyer de la Giroday, S. J. Dewhurst, N. Gisin, C. Y. Hu, F. Jelezko, S. Kroll, J. H. Muller, J. Nunn, E. S. Polzik, J. G. Rarity, H. De Riedmatten, W. Rosenfeld, A. J. Shields, N. Skoeld, R. M. Stevenson, R. Thew, I. A. Walmsley, M. C. Weber, H. Weinfurter, J. Wrachtrup, and R. J. Young. Quantum memories. *Eur. Phys. J. D*, 58(1):1–22, May 2010.

[113] Ö. E. Müstecaplioğlu. Quantum coherence and correlations of optical radiation by atomic ensembles interacting with a two-level atom in a microwave cavity. *Phys. Rev. A*, 83(2):023805, February 2011.

[114] S.C. Benjamin, B.W. Lovett, and J.W. Smith. Prospects for measurement-based quantum computing with solid state spins. *Laser & Photonics Rev.*, 3(6):556, 2009.

[115] David M. Toyli, Christoph D. Weis, Gregory D. Fuchs, Thomas Schenkel, and David D. Awschalom. Chip-scale nanofabrication of single spins and spin arrays in diamond. *Nano Lett.*, 10(8):3168–3172, August 2010.

[116] Hannes Bernien, Lilian Childress, Lucio Robledo, Matthew Markham, Daniel Twitchen, and Ronald Hanson. Two-photon quantum interference from separate nitrogen vacancy centers in diamond. *Phys. Rev. Lett.*, 108(4):043604, January 2012.

[117] A. Gruber, A. Drabenstedt, C. Tietz, L. Fleury, J. Wrachtrup, and C. vonBorczyskowski. Scanning confocal optical microscopy and magnetic resonance on single defect centers. *Science*, 276(5321):2012–2014, June 1997.

[118] Sota Kagami, Yutaka Shikano, and Koichiro Asahi. Detection and manipulation of single spin of nitrogen vacancy center in diamond toward application of weak measurement. *Physica E*, 43(3):761–765, January 2011.

[119] G. D. Fuchs, G. Burkard, P. V. Klimov, and D. D. Awschalom. A quantum memory intrinsic to single nitrogen-vacancy centres in diamond. *Nature Physics*, 7(10):789–793, October 2011.

[120] J. Kempe. Quantum random walks: an introductory overview. *Contemp. Phys.*, 44(4):307–327, August 2003.

[121] Salvador ElÃŋas Venegas-Andraca. Quantum walks: a comprehensive review. *Quant. Inf. Proc.*, 11(5):1015–1106, October 2012.

[122] Andris Ambainis. QUANTUM WALKS AND THEIR ALGORITHMIC APPLICATIONS. *Int. J. Quant. Inf.*, 01(04):507–518, December 2003.

[123] Yutaka Shikano. Special issue on quantum walks. *Quant. Inf. Proc.*, 11(5):1013–1014, October 2012.

[124] Takuya Kitagawa. Topological phenomena in quantum walks: elementary introduction to the physics of topological phases. *Quant. Inf. Proc.*, 11(5):1107–1148, October 2012.

[125] Y. Shikano. *J. Comp. Theor. Nanosci.*, In Press.

[126] Neil B. Lovett, Sally Cooper, Matthew Everitt, Matthew Trevers, and Viv Kendon. Universal quantum computation using the discrete-time quantum walk. *Phys. Rev. A*, 81(4):042330, April 2010.

[127] Pawel Kurzynski and Antoni Wojcik. Discrete-time quantum walk approach to state transfer. *Phys. Rev. A*, 83(6):062315, June 2011.

[128] Ö. E. Müstecaplioğlu. Quantum state transfer among crystallographic groups of nv centers in diamond. In *Society of Photo-Optical Instrumentation Engineers (SPIE) Conference Series*, volume 8069, page 9, 2011.

[129] B. C. Sanders, S. D. Bartlett, B. Tregenna, and P. L. Knight. Quantum quincunx in cavity quantum electrodynamics. *Phys. Rev. A*, 67(4):042305, April 2003.

[130] G. S. Agarwal and P. K. Pathak. Quantum random walk of the field in an externally driven cavity. *Phys. Rev. A*, 72(3):033815, September 2005.

[131] Peng Xue, Barry C. Sanders, Alexandre Blais, and Kevin Lalumiere. Quantum walks on circles in phase space via superconducting circuit quantum electrodynamics. *Phys. Rev. A*, 78(4):042334, October 2008.

[132] Lauri Lehman, Vaclav Zatloukal, Gavin K. Brennen, Jiannis K. Pachos, and Zhenghan Wang. Quantum walks with non-abelian anyons. *Phys. Rev. Lett.*, 106(23):230404, June 2011.

[133] C. M. Chandrashekar. Disordered-quantum-walk-induced localization of a bose-einstein condensate. *Phys. Rev. A*, 83(2):022320, February 2011.

[134] Sandeep K. Goyal, Filippus S. Roux, Andrew Forbes, and Thomas Konrad. Implementing quantum walks using orbital angular momentum of classical light. *arXiv:1211.1705*, November 2012.

[135] Linda Sansoni, Fabio Sciarrino, Giuseppe Vallone, Paolo Mataloni, Andrea Crespi, Roberta Ramponi, and Roberto Osellame. Two-particle bosonic-fermionic QuantumWalk via integrated photonics. *Phys. Rev. Lett.*, 108(1):010502, January 2012.

[136] H. Schmitz, R. Matjeschk, Ch Schneider, J. Glueckert, M. Enderlein, T. Huber, and T. Schaetz. Quantum walk of a trapped ion in phase space. *Phys. Rev. Lett.*, 103(9):090504, August 2009.

[137] J. F. Du, H. Li, X. D. Xu, M. J. Shi, J. H. Wu, X. Y. Zhou, and R. D. Han. Experimental implementation of the quantum random-walk algorithm. *Phys. Rev. A*, 67(4):042316, April 2003.

[138] Hagai B. Perets, Yoav Lahini, Francesca Pozzi, Marc Sorel, Roberto Morandotti, and Yaron Silberberg. Realization of quantum walks with negligible decoherence in waveguide lattices. *Phys. Rev. Lett.*, 100(17):170506, May 2008.

[139] M. A. Broome, A. Fedrizzi, B. P. Lanyon, I. Kassal, A. Aspuru-Guzik, and A. G. White. Discrete single-photon quantum walks with tunable decoherence. *Phys. Rev. Lett.*, 104(15):153602, April 2010.

[140] Takuya Kitagawa, Matthew A. Broome, Alessandro Fedrizzi, Mark S. Rudner, Erez Berg, Ivan Kassal, Alan Aspuru-Guzik, Eugene Demler, and Andrew G. White. Observation of topologically protected bound states in photonic quantum walks. *Nature Commun.*, 3, June 2012.

[141] D. Marcos, M. Wubs, J. M. Taylor, R. Aguado, M. D. Lukin, and A. S. Sorensen. Coupling nitrogen-vacancy centers in diamond to superconducting flux qubits. *Phys. Rev. Lett.*, 105(21):210501, November 2010.

[142] E. Vanoort, Nb Manson, and M. Glasbeek. Optically detected spin coherence of the diamond n-v center in its triplet ground-state. *J. Phys. C*, 21(23):4385–4391, August 1988.

[143] D. A. Redman, S. Brown, R. H. Sands, and S. C. Rand. Spin dynamics and electronic states of n-v centers in diamond by epr and 4-wave-mixing spectroscopy. *Phys. Rev. Lett.*, 67(24):3420–3423, December 1991.

[144] F. Jelezko and J. Wrachtrup. Single defect centres in diamond: A review. *Phys. Stat. Sol. (a)*, 203(13):3207–3225, October 2006.

[145] Benjamin Smeltzer, Lilian Childress, and Adam Gali. 13c hyperfine interactions in the nitrogen-vacancy centre in diamond. *New Journal of Physics*, 13(2):025021, 2011.

[146] JoHoNo Loubser and JoA van Wyk. Electron spin resonance in the study of diamond. *Reports on Progress in Physics*, 41(8):1201, 1978.

[147] MW Doherty, F Dolde, H Fedder, F Jelezko, J Wrachtrup, NB Manson, and LCL Hollenberg. Theory of the ground-state spin of the nv- center in diamond. *Physical Review B*, 85(20):205203, 2012.

[148] N. B. Manson, J. P. Harrison, and M. J. Sellars. Nitrogen-vacancy center in diamond: Model of the electronic structure and associated dynamics. *Phys. Rev. B*, 74(10):104303, September 2006.

[149] S. Sergei Gennadievich Ovchinnikov and V. V. Val'kov. *Hubbard Operators in the Theory of Stron*. Imperial College Press, 2004.

[150] T. P. Orlando, J. E. Mooij, L. Tian, C. H. van der Wal, L. S. Levitov, S. Lloyd, and J. J. Mazo. Superconducting persistent-current qubit. *Phys. Rev. B*, 60(22):15398–15413, December 1999.

[151] J. E. Mooij, T. P. Orlando, L. Levitov, L. Tian, C. H. van der Wal, and S. Lloyd. Josephson persistent-current qubit. *Science*, 285(5430):1036–1039, August 1999.

[152] P Forn-Díaz. PhD thesis, Delft University of Technology, 2010.

[153] F. G. Paauw, A. Fedorov, C. J. P. M. Harmans, and J. E. Mooij. Tuning the gap of a superconducting flux qubit. *Phys. Rev. Lett.*, 102(9):090501, March 2009.

[154] A. Fedorov, A. K. Feofanov, P. Macha, P. Forn-Diaz, C. J. P. M. Harmans, and J. E. Mooij. Strong coupling of a quantum oscillator to a flux qubit at its symmetry point. *Phys. Rev. Lett.*, 105(6):060503, August 2010.

[155] Xiaobo Zhu, Alexander Kemp, Shiro Saito, and Kouichi Semba. Coherent operation of a gap-tunable flux qubit. *Appl. Phys. Lett.*, 97(10):102503, September 2010.

[156] Xiaobo Zhu, Shiro Saito, Alexander Kemp, Kosuke Kakuyanagi, Shin-ichi Karimoto, Hayato Nakano, William J. Munro, Yasuhiro Tokura, Mark S. Everitt, Kae Nemoto, Makoto Kasu, Norikazu Mizuochi, and Kouichi Semba. Coherent coupling of a superconducting flux qubit to an electron spin ensemble in diamond. *Nature*, 478(7368):221–224, October 2011.

[157] P. Li and S. Q. Shen. Two-dimensional gapless spin liquids in frustrated SU(N) quantum magnets. *New J. Phys.*, 6:160, November 2004.

[158] S. Q. Shen and G. M. Zhang. Formation of energy gap in high-dimensional spin-orbital liquids. *Europhys. Lett.*, 57(2):274–280, January 2002.

[159] Bela Bauer, Philippe Corboz, Andreas M. LÃďuchli, Laura Messio, Karlo Penc, Matthias Troyer, and FrÃĺdÃĺric Mila. Three-sublattice order in the SU(3) heisenberg model on the square and triangular lattice. *Phys. Rev. B*, 85(12):125116, March 2012.

[160] B. R. Mollow and R. J. Glauber. Quantum theory of parametric amplification. i. *Phys. Rev.*, 160(5):1076–1096, August 1967.

[161] G. M. D'Ariano, M. G. A. Paris, and M. F. Sacchi. On the parametric approximation in quantum optics. *Nuovo Cimento*, 114(3):339–354, March 1999.

[162] T Holstein and Ho Primakoff. Field dependence of the intrinsic domain magnetization of a ferromagnet. *Physical Review*, 58(12):1098, 1940.

[163] Jr Morris and Bw Shore. Reduction of degenerate 2-level excitation to independent 2-state systems. *Phys. Rev. A*, 27(2):906–912, 1983.

[164] H. Fröhlich. Theory of the superconducting state. i. the ground state at the absolute zero of temperature. *Phys. Rev.*, 79(5):845–856, September 1950.

[165] J. R. Schrieffer and P. A. Wolff. Relation between the anderson and kondo hamiltonians. *Phys. Rev.*, 149(2):491–492, September 1966.

[166] S. Nakajima. Perturbation theory in statistical mechanics. *Advances in Physics*, 4(16):363–380, 1955.

[167] Alexandre Blais, Jay Gambetta, A. Wallraff, D. I. Schuster, S. M. Girvin, M. H. Devoret, and R. J. Schoelkopf. Quantum-information processing with circuit quantum electrodynamics. *Phys. Rev. A*, 75(3):032329, March 2007.

[168] Crispin Gardiner and Peter Zoller. *Quantum Noise: A Handbook of Markovian and Non-Markovian Quantum Stochastic Methods with Applications to Quantum Optics*. Springer, October 2004.

[169] J. R. Johansson, P. D. Nation, and Franco Nori. QuTiP: an open-source python framework for the dynamics of open quantum systems. *Comp. Phys. Comm.*, 183(8):1760–1772, August 2012.

[170] A. Shumovsky and Ö. E. Müstecaplioğlu. Conditions for observation of rabi oscillations in an exciton-polariton system. *Phys. Lett. A*, 209(1-2):88–94, December 1995.

[171] Leonard Mandel and Emil Wolf. *Optical Coherence and Quantum Optics*. Cambridge University Press, September 1995.

[172] Matthias Steffen, Shwetank Kumar, David P. DiVincenzo, J. R. Rozen, George A. Keefe, Mary Beth Rothwell, and Mark B. Ketchen. High-coherence hybrid superconducting qubit. *Phys. Rev. Lett.*, 105(10):100502, September 2010.

[173] Gopalakrishnan Balasubramanian, Philipp Neumann, Daniel Twitchen, Matthew Markham, Roman Kolesov, Norikazu Mizuochi, Junichi Isoya, Jocelyn Achard, Johannes Beck, Julia Tissler, Vincent Jacques, Philip R. Hemmer, Fedor Jelezko, and Joerg Wrachtrup. Ultralong spin coherence time in isotopically engineered diamond. *Nature Mat.*, 8(5):383–387, May 2009.

[174] F. Yoshihara, K. Harrabi, A. O. Niskanen, Y. Nakamura, and J. S. Tsai. Decoherence of flux qubits due to 1/f flux noise. *Phys. Rev. Lett.*, 97(16):167001, October 2006.

[175] K. Kakuyanagi, T. Meno, S. Saito, H. Nakano, K. Semba, H. Takayanagi, F. Deppe, and A. Shnirman. Dephasing of a superconducting flux qubit. *Phys. Rev. Lett.*, 98(4):047004, January 2007.

[176] A. S. Holevo. *Lecture Notes in Mathematics*. Springer, Berlin, 1984.

[177] DW Berry and Howard Mark Wiseman. Optimal states and almost optimal adaptive measurements for quantum interferometry. *Physical review letters*, 85(24):5098, 2000.

[178] Emilio Bagan, Alex Monras, and Ramon Munoz-Tapia. Phase variance of squeezed vacuum states. *Physical Review A*, 78(4):043829, 2008.

[179] Murray Gell-Mann and Abraham Pais. Behavior of neutral particles under charge conjugation. *Physical Review*, 97(5):1387, 1955.

[180] CP Sun, Y Li, and XF Liu. Quasi-spin-wave quantum memories with a dynamical symmetry. *Physical review letters*, 91(14):147903, 2003.

[181] Zoltan Kurucz, JH Wesenberg, and Klaus Mølmer. Spectroscopic properties of inhomogeneously broadened spin ensembles in a cavity. *Physical Review A*, 83(5):053852, 2011.